ARTICLE

Design, synthesis and pharmacological characterization of N-(3-ethylbenzo[d]isoxazol-5-yl) sulfonamide derivatives as BRD4 inhibitors against acute myeloid leukemia

Mao-feng Zhang[1], Xiao-yu Luo[2], Cheng Zhang[3], Chao Wang[3,4], Xi-shan Wu[3], Qiu-ping Xiang[3], Yong Xu[3,5,6] and Yan Zhang[3]

BRD4 plays a key role in the regulation of gene transcription and has been identified as an attractive target for cancer treatment. In this study, we designed 26 new compounds by modifying 3-ethyl-benzo[d]isoxazole core with sulfonamides. Most compounds exhibited potent BRD4 binding activities with ΔT_m values exceeding 6 °C. Two crystal structures of **11h** and **11r** in complex with BRD4(1) were obtained to characterize the binding patterns. Compounds **11h** and **11r** were effective for BRD4(1) binding and showed remarkable anti-proliferative activity against MV4-11 cells with IC_{50} values of 0.78 and 0.87 μM. Furthermore, **11r** (0.5−10 μM) concentration-dependently inhibited the expression levels of oncogenes including c-Myc and CDK6 in MV4-11 cells. Moreover, **11r** (0.5−10 μM) concentration-dependently blocked cell cycle in MV4-11 cells at G_0/G_1 phase and induced cell apoptosis. Compound **11r** may serve as a new lead compound for further drug development.

Keywords: acute myeloid leukemia; BRD4 inhibitors; 3-ethyl-benzo[d]isoxazole; c-Myc; CDK6; apoptosis

INTRODUCTION
Bromodomain and extra-terminal (BET) family consists of four members including BRD2, BRD3, BRD4, and BRDT. All the BET proteins contain two structurally similar bromodomains (BD1 and BD2), which can bind to acetyl-lysine (K_{Ac}) residues on histone tails of chromatin. Thus, the bromodomain-containing proteins act as epigenetic "readers" by binding to K_{Ac} via the bromodomain to regulate gene expression [1]. Each bromodomain has two loop regions (ZA and BC loops) [2] and a hydrophobic area named as "WPF shelf" [3]. The entire structure constitutes the K_{Ac} binding site.

BRD4 is a well-studied member of BET family. It can recruit the positive transcription elongation factor b (P-TEFb) to the promoter and activate RNA polymerase II [4, 5]. In addition, BRD4 can promote the transcription of key genes (Bcl-2, c-Myc and CDK6) [6–8], which plays an essential role in the proliferation and cell cycle progression of tumor cells. Therefore, the expression of key oncogenes can be inhibited through the displacement of BRD4 from chromatin. Accumulative evidence indicates that BRD4 protein has been implicated in various human diseases, including acute myeloid leukemia (AML) [8–10], prostate cancer [11, 12], breast cancer [13–15], gastrointestinal stromal tumor (GIST) [16], neuroblastoma [17], pancreatic cancer [18, 19], cholangiocarcinoma [20] as well as inflammations [21, 22].

Multiple BRD4 inhibitors have been reported by researchers, some of which are undergoing clinical trials for cancer therapy.

(+)-JQ1 (**1**, Fig. 1) was the first potent BRD4 bromodomain inhibitor with a triazolothienodiazepine skeleton [23], which was widely used as a probe to explore the biological function of BET proteins in treatment of various human diseases. The structurally related derivatives OTX-015 (Supplementary Fig. S1a) [24] and I-BET762 (Supplementary Fig. S1b) [25] have completed the phase 1 clinical trials for malignancies. 3,5-Dimethylisoxazole was another preferred scaffold, which was firstly reported by Hewings [26]. The scaffold has been used for the design of different BRD4 inhibitors (Supplementary Fig. S1c and S1d) [27, 28]. The representative inhibitor I-BET151 (**2**, Fig. 1) discovered by GSK was reported for the treatment of MLL-fusion leukemia [6]. In addition, several BRD4 inhibitors with different scaffolds, such as PFI-1 (**3**, Fig. 1) [29, 30], 2-thiazolidinone derivative (Supplementary Fig. S1e) [31], ABBV-075 (Supplementary Fig. S1f) [32] and CPI-0610 (Supplementary Fig. S1g) [33], are undergoing clinical trials for solid tumor and lymphoma with encouraging data. We previously reported two class of BET bromodomain inhibitors containing a benzo[cd]indol-2 (1H)-one structure (Supplementary Fig. S1h) [34] and a 3-methyl-benzo[d]isoxazole scaffold (Y06036, **4**, Fig. 1) [35], respectively. Compound **4** demonstrated potent and selective binding affinities to BET proteins with good in vitro and in vivo efficacy against prostate cancer [35]. The X-ray diffraction of **4**-BRD4 crystal structure also provided solid evidence for further structure-based optimization. Despite the structural differences of various inhibitors, they share similar warheads that can mimic the K_{Ac}.

[1]College of Pharmacy, Taizhou Polytechnic College, Taizhou 225300, China; [2]Guangzhou Younan Technology Co., Ltd, Guangzhou 510663, China; [3]Center for Chemical Biology and Drug Discovery, Guangzhou Institutes of Biomedicine and Health, Chinese Academy of Sciences, Guangzhou 510530, China; [4]University of Chinese Academy of Sciences, Beijing 100049, China; [5]State Key Laboratory of Respiratory Disease, Guangzhou Institutes of Biomedicine and Health, Chinese Academy of Sciences, Guangzhou 510530, China and [6]China-New Zealand Joint Laboratory on Biomedicine and Health, Guangzhou 510530, China
Correspondence: Mao-feng Zhang (zhang_maofeng@163.com) or Yong Xu (xu_yong@gibh.ac.cn) or Yan Zhang (zhang_yan2012@gibh.ac.cn)
These authors contributed equally: Mao-feng Zhang, Xiao-yu Luo
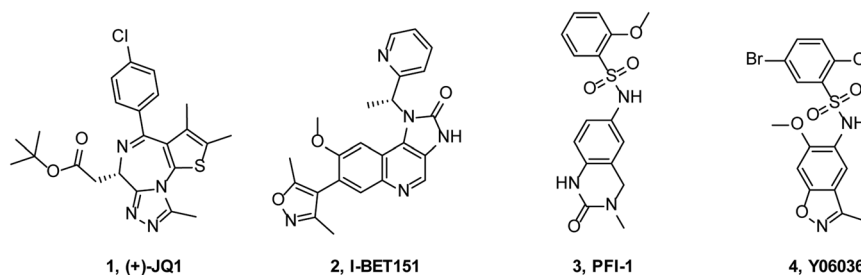
Fig. 1 Chemical structures of representative BRD4 inhibitors. The listed inhibitors were (+)-JQ1 (**1**), I-BET151 (**2**), PFI-1 (**3**) and Y06036 (**4**).

BRD4 inhibitors are undoubtedly potential anticancer drugs. However, the existing inhibitors are often accompanied by side effects of thrombocytopenia, fatigue, and diarrhoea [36]. None of the BRD4 inhibitors received approval in the past decade, which meant there was no obvious "low-hanging fruit" of their development. Besides, BRD inhibitors are not the "magic bullet" for treatment of all cancers as we expected and they are likely to work in selective cancer types [36]. Different chemical structures may cause nuances for BRD inhibition and show different effect in tumor types or toxicity profile. Enriching the structural library of inhibitors and performing rational combinations may be a potential direction for the research of BET inhibitors in the future. Thus, the development of new BRD4 inhibitors still attracts attentions. The fine structure-activity relationships (SARs) are needed to explore for providing inhibitors with different cellular pharmacological profiles and clinical application. In this work, we report the design and evaluation of a class of new BRD4 inhibitors with a 3-ethyl-benzo[d]isoxazole scaffold for potential treatment of AML. The biological functions of the compounds were evaluated by thermal shift assay, crystallography analysis, cell viability assay, RT-PCR technology, Western bolt and flow cytometry.

MATERIALS AND METHODS
Chemistry
The reagents and solvents were purchased from commercial sources and used without further purification. ^{1}H NMR and ^{13}C NMR spectra were recorded on Bruker Avance 400 MHz spectrometer (Bruker, Karlsruhe, Germany) with DMSO-d_6 or CDCl$_3$ as the solvent. Chemical shifts are given in ppm throughout. Coupling constants (J) are expressed in hertz (Hz). NMR chemical shifts (δ) are reported in parts per million (ppm) units. The high-resolution mass spectra were performed on a UPLC G2-XS QTOF mass spectrometer (Waters, Milford, MA, USA). TLC analysis was performed on GF254 silica gel plates (Qingdao Haiyang Chemical, China) under ZF-20D UV light (254 nm) (Yuhua instrument, Gongyi, China) or I$_2$ in silica gel for monitoring all reactions. Flash column chromatography was performed on silica gel (300–400 mesh). Melting point was measured (uncorrected) on X-6 melting point apparatus (Beijing Tech, China). Purity of all compounds was determined by LC-20AT prominence high-performance liquid chromatography (HPLC) (SHIMADZU, Kyoto, Japan) using an InertSustain C18 column (150 mm × 4.6 mm, 5 μm) with the 65% solvent A (MeOH) and 35% solvent B (H$_2$O) as eluents. The flow rate was set as 0.8 mL/min and the signals were monitored by a SPD-20A prominence UV/VIS detector at 254 nm. The purity of all the final compounds was determined by HPLC to be >97%.

N-(4-hydroxy-2-methoxy-5-propionylphenyl)acetamide (7)
N-(2, 4-dimethoxyphenyl) acetamide **6** (13.0 g, 66.6 mmol, synthesized according to previous procedure [35]) and propionyl chloride (18.5 g, 199.8 mmol) was dissolved in DCM (40 mL). Anhydrous AlCl$_3$ (35.5 g, 266.4 mmol) was added in portions with vigorous stirring under ice-cooling. The reaction temperature was raised to

43 °C and stirred for 3 h. After the reaction was completed, the mixture was slowly added dropwise to crushed ice with stirring. The organic layer was separated, and the solvent was evaporated under reduced pressure. Dilute hydrochloric acid was added dropwise to the residue and the mixture was stirred for 0.5 h. The solid was filtered and washed with hydrochloric acid and water, and then dried to obtain the target compound as a pale green solid (12.8 g, 81.0% yield). ^{1}H NMR (400 MHz, DMSO-d_6), δ: 12.57 (s, 1H, OH), 9.19 (brs, 1H, NH), 8.30 (s, 1H, ArH), 6.58 (s, 1H, ArH), 3.87 (s, 3H, OCH$_3$), 2.95 (q, J = 7.2 Hz, 2H, CH$_2$CH$_3$), 2.05 (s, 3H, COCH$_3$), 1.09 (t, J = 7.2 Hz, 3H, CH$_2$CH$_3$); MS (ESI), m/z: 238.1 [M + H]$^+$.

N-(4-hydroxy-5-(1-(hydroxyimino)propyl)-2-methoxyphenyl)acetamide (8)
Compound **7** (11.0 g, 46.4 mmol), hydroxylamine hydrochloride (6.4 g, 92.7 mmol) and anhydrous sodium acetate (7.6 g, 92.7 mmol) was dissolved in 130 mL of a mixed solvent of ethanol and water (anhydrous ethanol: water = 7: 3, v/v). The mixture was warmed to 80 °C and stirred under reflux for 2 h. After the reaction was completed, the mixture was cooled to room temperature. The mixture was concentrated under reduced pressure to precipitate a solid. Water (100 mL) was then added, and the solid was filtered, washed and dried to obtain the title compound as a pale green solid (10.1 g, 86.4% yield). ^{1}H NMR (400 MHz, DMSO-d_6), δ: 11.80 (s, 1H, OH), 11.31 (s, 1H, OH), 9.07 (brs, 1H, NH), 7.87 (s, 1H, 3-ArH), 6.55 (s, 1H, 6-ArH), 3.80 (s, 3H, OCH$_3$), 2.70 (q, J = 7.5 Hz, 2H, CH$_2$CH$_3$), 2.03 (s, 3H, COCH$_3$), 1.08 (t, J = 7.5 Hz, 3H, CH$_2$CH$_3$); MS (ESI), m/z: 253.1 [M + H]$^+$.

N-(3-ethyl-6-methoxybenzo[d]isoxazol-5-yl)acetamide (9)
Compound **8** (10.5 g, 41.6 mmol) was dissolved in 1, 4-dioxane (45 mL). Next, 24 mL of N, N-dimethylformamide dimethyl acetal (DMF-DMA) was added slowly to the mixture with vigorous stirring. The temperature was raised to 100 °C and stirred for 10 min. After the reaction was completed, dilute hydrochloric acid (50 mL) and water (180 mL) was added to the mixture with stirring to precipitate a solid. The solid was washed and dried to obtain the target compound as a pale green solid (5.5 g, 56.4% yield). ^{1}H NMR (400 MHz, DMSO-d_6), δ: 9.29 (brs, 1H, NH), 8.27 (s, 1H, 7-ArH), 7.37 (s, 1H, 3-ArH), 3.93 (s, 3H, OCH$_3$), 2.91 (q, J = 7.6 Hz, 2H, CH$_2$CH$_3$), 2.11 (s, 3H, COCH$_3$), 1.30 (t, J = 7.6 Hz, 3H, CH$_2$CH$_3$); MS (ESI), m/z: 235.1 [M + H]$^+$.

3-Ethyl-6-methoxybenzo[d]isoxazol-5-amine (10)
Compound **9** (5.0 g, 21.3 mmol) was added to hydrochloric acid (120 mL, 3 mol/L). The reaction mixture was stirred at 90 °C for 3 h. After the reaction was completed, the sodium hydroxide solution was added to adjust the pH to 7–9, which allow the precipitation of a solid. The product was filtered, and the cake was washed with water, dried to obtain the target compound as a brown solid (3.8 g, 92.6% yield). ^{1}H NMR (400 MHz, CDCl$_3$), δ: 6.92 (s, 1H, 7-ArH)), 6.82 (s, 1H, 4-ArH), 3.92 (s, 3H, OCH$_3$), 3.85 (brs, 2H, NH$_2$), 2.89 (q, J = 7.6 Hz, 2H, CH$_2$CH$_3$), 1.38 (t, J = 7.6 Hz, 3H, CH$_2$CH$_3$); ^{13}C NMR (101 MHz, CDCl$_3$) δ 159.00, 158.75, 151.19, 133.75, 113.77, 102.82, 91.52, 55.91, 18.90, 12.19; MS (ESI), m/z: 193.1 [M + H]$^+$.

General procedure for the synthesis of 3-ethyl-benzo[d]isoxazol-containing sulfonamides 11

To a solution of DCM (6 mL) was added compound **10** (65 mg, 0.34 mmol), sulfonyl chloride (0.41 mmol) and pyridine (0.3 mL). The resulting mixture was stirred at 43 °C for 3–12 h. The reaction was monitored by TLC (ethyl acetate/petroleum ether (1:1, v/v)). On completion of the reaction, the mixture was diluted with 1 mol/L HCl (8 mL) and water (15 mL) and extracted with ethyl acetate (3 × 20 mL). The separated organic phase was washed with water and brine, dried over anhydrous Na_2SO_4 and evaporated under reduced pressure. The residue was purified by flash chromatography on silica gel to give the title compound as a solid.

N-(3-Ethyl-6-methoxybenzo[d]isoxazol-5-yl)ethanesulfonamide (11a)

White solid; yield: 54.9%; m.p.: 122–123 °C; ^1H NMR (400 MHz, CDCl$_3$) δ 7.77 (s, 1H, 7-ArH), 7.05 (s, 1H, 4-ArH), 6.78 (brs, 1H, SO$_2$NH), 3.99 (s, 3H, OCH$_3$), 3.04 (q, J = 7.4 Hz, 2H, SO$_2$CH$_2$CH$_3$), 2.96 (q, J = 7.6 Hz, 2H, 3-CH$_2$CH$_3$), 1.41 (t, J = 7.6 Hz, 3H, 3-CH$_2$CH$_3$), 1.34 (t, J = 7.4 Hz, 3H, SO$_2$CH$_2$CH$_3$); ^{13}C NMR (101 MHz, CDCl$_3$) δ 161.35, 159.85, 152.37, 123.45, 114.51, 112.75, 92.22, 56.51, 45.51, 18.84, 12.11, 8.12; HRMS (ESI) m/z calcd for C$_{12}$H$_{16}$N$_2$O$_4$S [M + H]$^+$: 285.0831; found: 285.0912. HPLC, t_R = 4.278 min, 98.91% purity.

N-(3-Ethyl-6-methoxybenzo[d]isoxazol-5-yl)propane-1-sulfonamide (11b)

White solid; yield: 39.4%; m.p.: 108–109 °C; ^1H NMR (400 MHz, CDCl$_3$) δ 7.76 (s, 1H, 7-ArH), 7.05 (s, 1H, 4-ArH), 6.76 (s, 1H, SO$_2$NH), 3.99 (s, 3H, OCH$_3$), 3.05 – 2.90 (m, 4H, SO$_2$CH$_2$, 3-CH$_2$CH$_3$), 1.88 – 1.76 (m, 2H, SO$_2$CH$_2$CH$_2$), 1.41 (t, J = 7.5 Hz, 3H, 3-CH$_2$CH$_3$), 0.99 (t, J = 7.4 Hz, 3H, CH$_2$CH$_2$CH$_3$); ^{13}C NMR (101 MHz, CDCl$_3$) δ 161.35, 159.87, 152.40, 123.49, 114.53, 112.75, 92.22, 56.52, 52.94, 18.85, 17.20, 12.92, 12.11; HRMS (ESI) m/z calcd for C$_{13}$H$_{18}$N$_2$O$_4$S [M + H]$^+$: 299.0987; found: 299.1067. HPLC, t_R = 5.636 min, 98.36% purity.

N-(3-Ethyl-6-methoxybenzo[d]isoxazol-5-yl)butane-1-sulfonamide (11c)

White solid; yield: 48%; m.p.: 100–101 °C; ^1H NMR (400 MHz, CDCl$_3$) δ 7.76 (s, 1H, 7-ArH), 7.05 (s, 1H, 4-ArH), 6.76 (s, 1H, SO$_2$NH), 3.99 (s, 3H, OCH$_3$), 3.10 – 2.85 (m, 4H, SO$_2$CH$_2$, 3-CH$_2$CH$_3$), 1.85 – 1.75 (m, 2H, SO$_2$CH$_2$CH$_2$), 1.51 – 1.28 (m, 5H, 3-CH$_2$CH$_3$, SO$_2$CH$_2$CH$_2$CH$_2$), 0.88 (t, J = 7.0 Hz, 3H, CH$_2$CH$_2$CH$_3$); ^{13}C NMR (101 MHz, CDCl$_3$) δ 161.36, 159.88, 152.39, 123.49, 114.53, 112.79, 92.21, 56.48, 50.94, 25.41, 21.44, 18.85, 13.56, 12.11; HRMS (ESI) m/z calcd for C$_{14}$H$_{20}$N$_2$O$_4$S [M + H]$^+$: 313.1144; found: 313.1224. HPLC, t_R = 8.027 min, 99.03% purity.

N-(3-Ethyl-6-methoxybenzo[d]isoxazol-5-yl)benzenesulfonamide (11d)

White solid; yield: 47.8%; m.p.: 169–170 °C; ^1H NMR (400 MHz, CDCl$_3$) δ 7.78 (s, 1H, ArH), 7.74 – 7.56 (m, 2H, phenyl ArH), 7.56 – 7.30 (m, 3H, phenyl ArH), 6.91 (brs, 1H, SO$_2$NH), 6.81 (s, 1H, 4-ArH), 3.62 (s, 3H, OCH$_3$), 2.97 (d, J = 5.5 Hz, 2H, 3-CH$_2$CH$_3$), 1.42 (s, 3H, 3-CH$_2$CH$_3$); ^{13}C NMR (101 MHz, CDCl$_3$) δ 161.74, 159.90, 153.16, 138.80, 133.05, 128.77 (2×C), 127.22 (2×C), 122.92, 114.87, 114.36, 91.94, 56.12, 18.88, 12.121; HRMS (ESI) m/z calcd for C$_{16}$H$_{16}$N$_2$O$_4$S [M + H]$^+$: 333.0831; found: 333.0916. HPLC, t_R = 6.890 min, 97.76% purity.

N-(3-Ethyl-6-methoxybenzo[d]isoxazol-5-yl)-2-fluorobenzenesulfonamide (11e)

White solid; yield: 54.4%; m.p.: 179–180 °C; ^1H NMR (400 MHz, CDCl$_3$) δ 7.73 (d, J = 7.4 Hz, 2H, 6'-ArH, 7-ArH), 7.58 – 7.43 (m, 1H, 4'-ArH), 7.29 (brs, 1H, SO$_2$NH), 7.20 – 7.07 (m, 2H, 3', 5'-ArH), 6.85 (s, 1H, 4-ArH), 3.77 (s, 3H, OCH$_3$), 2.94 (q, J = 7.5 Hz, 2H, 3-CH$_2$CH$_3$), 1.39 (t, J = 7.5 Hz, 3H, 3-CH$_2$CH$_3$); ^{13}C NMR (101 MHz, CDCl$_3$) δ 161.60, 160.36 (d, J = 257.6 Hz, F-2'-ArC), 159.83, 157.81 (d, J = 257.6 Hz, F-2'-ArC), 153.03, 135.54 (d, J = 9.1 Hz, F-4'-ArC), 135.45 (d, J = 9.1 Hz, F-4'-ArC), 130.90, 126.83 (d, J = 13.1 Hz, F-1'-ArC),

126.70 (d, J = 13.1 Hz, F-1'-ArC), 124.17 (d, J = 4.0 Hz, F-6'-ArC), 124.13 (d, J = 4.0 Hz, F-6'-ArC), 122.48, 116.87 (d, J = 21.2 Hz, F-3'-ArC), 116.66 (d, J = 21.2 Hz, F-3'-ArC), 114.26, 114.23, 91.90, 56.18, 18.82, 12.09; HRMS (ESI) m/z calcd for C$_{16}$H$_{15}$FN$_2$O$_4$S [M + H]$^+$: 351.0737; found: 351.0817. HPLC, t_R = 6.538 min, 98.90% purity.

2-Chloro-N-(3-ethyl-6-methoxybenzo[d]isoxazol-5-yl)benzenesulfonamide (11f)

White solid; yield: 54.4%; m.p.: 121–122 °C; ^1H NMR (400 MHz, CDCl$_3$) δ 7.93 (dd, J = 7.9, 1.3 Hz, 1H, 6'-ArH), 7.70 (s, 1H, 7-ArH), 7.55 (brs, 1H, SO$_2$NH), 7.51 – 7.46 (m, 1H, 3'-ArH), 7.43 (td, J = 7.7, 1.4 Hz, 1H, 4'-ArH), 7.30 – 7.24 (m, 1H, 5'-ArH), 6.85 (s, 1H, 4-ArH), 3.78 (s, 3H, OCH$_3$), 2.93 (q, J = 7.6 Hz, 2H, 3-CH$_2$CH$_3$), 1.38 (t, J = 7.6 Hz, 3H, 3-CH$_2$CH$_3$); ^{13}C NMR (101 MHz, CDCl$_3$) δ 161.45, 159.78, 152.83, 136.24, 134.10, 132.06, 131.81, 131.61, 126.81, 122.62, 114.19, 113.57, 91.93, 56.13, 18.81, 12.10; HRMS (ESI) m/z calcd for C$_{16}$H$_{15}$ClN$_2$O$_4$S [M + H]$^+$: 367.0441; found: 367.0522. HPLC, t_R = 8.824 min, 98.63% purity.

2-Bromo-N-(3-ethyl-6-methoxybenzo[d]isoxazol-5-yl)benzenesulfonamide (11g)

White solid; yield: 64.7%; m.p.: 142–143 °C; ^1H NMR (400 MHz, CDCl$_3$) δ 8.00 – 7.93 (m, 1H, 3'-ArH), 7.73 – 7.67 (m, 2H, 7-ArH, 6'-ArH), 7.64 (brs, 1H, SO$_2$NH), 7.38 – 7.28 (m, 2H, 4', 5'-ArH), 6.85 (s, 1H, 4-ArH), 3.78 (s, 3H, OCH$_3$), 2.93 (q, J = 7.6 Hz, 2H, 3-CH$_2$CH$_3$), 1.38 (t, J = 7.6 Hz, 3H, 3-CH$_2$CH$_3$); ^{13}C NMR (101 MHz, CDCl$_3$) δ 161.46, 159.78, 152.84, 137.96, 135.14, 134.04, 132.04, 127.39, 122.63, 120.31, 114.18, 113.61, 91.94, 56.08, 18.82, 12.11; HRMS (ESI) m/z calcd for C$_{16}$H$_{15}$BrN$_2$O$_4$S [M + H]$^+$: 410.9936 & 412.9915; found: 411.0012 & 412.9994. HPLC, t_R = 10.020 min, 98.18% purity.

N-(3-Ethyl-6-methoxybenzo[d]isoxazol-5-yl)-2-methoxybenzenesulfonamide (11h)

White solid; yield: 71.7%; m.p.: 142–143 °C; ^1H NMR (400 MHz, CDCl$_3$) δ 7.82 (d, J = 7.6 Hz, 1H, 6'-ArH), 7.72 (s, 1H, 7-ArH), 7.59 (brs, 1H, SO$_2$NH), 7.45 (t, J = 7.7 Hz, 1H, 4'-ArH), 7.00 – 6.90 (m, 2H, 3', 5'-ArH), 6.86 (s, 1H, 4-ArH), 3.96 (s, 3H, 2'-OCH$_3$), 3.83 (s, 3H, 6-OCH$_3$), 2.91 (q, J = 7.5 Hz, 2H, 3-CH$_2$CH$_3$), 1.36 (t, J = 7.5 Hz, 3H, 3-CH$_2$CH$_3$); ^{13}C NMR (101 MHz, CDCl$_3$) δ 160.91, 159.81, 156.45, 152.21, 135.05, 130.94, 126.20, 123.72, 120.27, 114.21, 111.97, 111.80, 91.81, 56.35, 56.10, 18.79, 12.10; HRMS (ESI) m/z calcd for C$_{17}$H$_{18}$N$_2$O$_5$S [M + H]$^+$: 363.0936; found: 363.1018. HPLC, t_R = 7.302 min, 97.86% purity.

N-(3-Ethyl-6-methoxybenzo[d]isoxazol-5-yl)-2-(trifluoromethoxy)benzenesulfonamide (11i)

White solid; yield: 67.9%; m.p.: 92–93 °C; ^1H NMR (400 MHz, CDCl$_3$) δ 7.90 (dd, J = 7.9, 1.5 Hz, 1H, 6'-ArH), 7.73 (s, 1H, 7-ArH), 7.55 (td, J = 8.4, 1.6 Hz, 1H, 4'-ArH), 7.38 – 7.30 (m, 2H, SO$_2$NH, 3'-ArH), 7.26 (td, J = 8.0, 0.8 Hz, 1H, 5'-ArH), 6.87 (s, 1H, 4-ArH), 3.79 (s, 3H, OCH$_3$), 2.93 (q, J = 7.6 Hz, 2H, 3-CH$_2$CH$_3$), 1.38 (t, J = 7.6 Hz, 3H, 3-CH$_2$CH$_3$); ^{13}C NMR (101 MHz, CDCl$_3$) δ 161.43, 159.82, 152.61, 146.22, 134.92, 131.69, 130.09, 125.90, 124.16 (q, J = 262.6 Hz, OCF$_3$), 122.56, 121.56 (q, J = 262.6 Hz, OCF$_3$), 118.97 (q, J = 262.6 Hz, OCF$_3$), 118.95, 116.37 (q, J = 262.6 Hz, OCF$_3$), 114.24, 113.24, 91.89, 56.13, 18.81, 12.10; HRMS (ESI) m/z calcd for C$_{17}$H$_{15}$F$_3$N$_2$O$_5$S [M + H]$^+$: 417.0654; found: 417.0735. HPLC, t_R = 11.895 min, 99.20% purity.

3-Chloro-N-(3-ethyl-6-methoxybenzo[d]isoxazol-5-yl)benzenesulfonamide (11j)

White solid; yield: 53.5%; m.p.: 152–153 °C; ^1H NMR (400 MHz, CDCl$_3$) δ 7.77 (s, 1H, 7-ArH), 7.73 (s, 1H, 2'-ArH), 7.51 (d, J = 7.8 Hz, 1H, 6'-ArH), 7.47 (d, J = 8.1 Hz, 1H, 4'-ArH), 7.30 (t, J = 7.9 Hz, 1H, 5'-ArH), 6.95 (brs, 1H, SO$_2$NH), 6.85 (s, 1H, 4-ArH), 3.68 (s, 3H, OCH$_3$), 2.98 (q, J = 7.6 Hz, 2H, 3-CH$_2$CH$_3$), 1.43 (t, J = 7.6 Hz, 3H, 3-CH$_2$CH$_3$); ^{13}C NMR (101 MHz, CDCl$_3$) δ 161.91, 159.89, 153.22, 140.49, 135.01, 133.12, 130.00, 127.35, 125.39, 122.34, 115.35, 114.45, 92.06, 56.19,

18.87, 12.12; HRMS (ESI) m/z calcd for $C_{16}H_{15}ClN_2O_4S$ $[M + H]^+$: 367.0441; found: 367.0518. HPLC, t_R = 12.235 min, 98.62% purity.

3-Bromo-N-(3-ethyl-6-methoxybenzo[d]isoxazol-5-yl) benzenesulfonamide (11k)
White solid; yield: 70.7%; m.p.: 160–161 °C; ^{1}H NMR (400 MHz, CDCl$_3$) δ 7.89 (s, 1H, 2′-ArH), 7.77 (s, 1H, 7-ArH), 7.62 (d, J = 7.8 Hz, 1H, 6′-ArH), 7.55 (d, J = 7.7 Hz, 1H, 4′-ArH), 7.23 (t, J = 8.0 Hz, 1H, 5′-ArH), 6.96 (brs, 1H, SO$_2$NH), 6.85 (s, 1H, 4-ArH), 3.68 (s, 3H, OCH$_3$), 2.98 (q, J = 7.5 Hz, 2H, 3-CH$_2$CH$_3$), 1.43 (t, J = 7.5 Hz, 3H, 3-CH$_2$CH$_3$); ^{13}C NMR (101 MHz, CDCl$_3$) δ 161.93, 159.88, 153.25, 140.61, 136.00, 130.20, 130.19, 125.82, 122.71, 122.31, 115.45, 114.44, 92.06, 56.21, 18.87, 12.13; HRMS (ESI) m/z calcd for $C_{16}H_{15}BrN_2O_4S$ $[M + H]^+$: 410.9936 & 412.9915; found: 411.0017 & 412.9996. HPLC, t_R = 13.004 min, 97.46% purity.

5-Chloro-N-(3-ethyl-6-methoxybenzo[d]isoxazol-5-yl)-2-methoxybenzenesulfonamide (11l)
White solid; yield: 71.4%; m.p.: 157–158 °C; ^{1}H NMR (400 MHz, CDCl$_3$) δ 7.80 (d, J = 2.4 Hz, 1H, 6′-ArH), 7.72 (s, 1H, 7-ArH), 7.57 (brs, 1H, SO$_2$NH), 7.40 (dd, J = 8.8, 2.4 Hz, 1H, 4′-ArH), 6.94 – 6.84 (m, 2H, 4-ArH, 3′-ArH), 3.95 (s, 3H, 2′-OCH$_3$), 3.84 (s, 3H, 6-OCH$_3$), 2.94 (q, J = 7.6 Hz, 2H, 3-CH$_2$CH$_3$), 1.38 (t, J = 7.6 Hz, 3H, 3-CH$_2$CH$_3$); ^{13}C NMR (101 MHz, CDCl$_3$) δ 161.07, 159.85, 155.03, 152.24, 134.64, 130.52, 127.69, 125.57, 123.21, 114.34, 113.20, 112.46, 91.96, 56.50, 56.39, 18.81, 12.10; HRMS (ESI) m/z calcd for $C_{17}H_{17}ClN_2O_5S$ $[M + H]^+$: 397.0547; found: 397.0625. HPLC, t_R = 13.742 min, 98.46% purity.

5-Bromo-N-(3-ethyl-6-methoxybenzo[d]isoxazol-5-yl)-2-methoxybenzenesulfonamide (11m)
White solid; yield: 43.5%; m.p.: 167–168 °C; ^{1}H NMR (400 MHz, CDCl$_3$) δ 7.94 (d, J = 2.4 Hz, 1H, 6′-ArH), 7.72 (s, 1H, 7-ArH), 7.60 – 7.50 (m, 2H, SO$_2$NH, 4′-ArH), 6.89 (s, 1H, 4-ArH), 6.83 (d, J = 8.8 Hz, 1H, 3′-ArH), 3.94 (s, 3H, 2′-OCH$_3$), 3.84 (s, 3H, 6-OCH$_3$), 2.94 (q, J = 7.6 Hz, 2H, 3-CH$_2$CH$_3$), 1.39 (t, J = 7.6 Hz, 3H, 3-CH$_2$CH$_3$); ^{13}C NMR (101 MHz, CDCl$_3$) δ 161.07, 159.87, 155.53, 152.21, 137.59, 133.31, 128.05, 123.21, 114.38, 113.63, 112.43 (2×C), 91.98, 56.46, 56.40, 18.84, 12.15; HRMS (ESI) m/z calcd for $C_{17}H_{17}BrN_2O_5S$ $[M + H]^+$: 441.0042 & 443.0021; found: 441.0125 & 443.0107. HPLC, t_R = 15.044 min, 99.11% purity.

5-Bromo-N-(3-ethyl-6-methoxybenzo[d]isoxazol-5-yl)-2,3-dihydrobenzofuran-7-sulfonamide (11n)
White solid; yield: 84.0%; m.p.: 152–153 °C; ^{1}H NMR (400 MHz, CDCl$_3$) δ 7.70 (s, 1H, 7-ArH), 7.64 (d, J = 1.5 Hz, 1H, 6′-ArH), 7.41 (brs, 1H, SO$_2$NH), 7.39 (d, J = 1.5 Hz, 1H, 4′-ArH), 6.90 (s, 1H, 4-ArH), 4.70 (t, J = 8.8 Hz, 2H, OCH$_2$CH$_2$), 3.84 (s, 3H, OCH$_3$), 3.21 (t, J = 8.8 Hz, 2H, OCH$_2$CH$_2$), 2.94 (q, J = 7.6 Hz, 2H, 3-CH$_2$CH$_3$), 1.39 (t, J = 7.6 Hz, 3H, 3-CH$_2$CH$_3$); ^{13}C NMR (101 MHz, CDCl$_3$) δ 161.11, 159.87, 156.13, 152.23, 132.86, 131.98, 130.16, 123.08, 121.76, 114.26, 112.09, 111.71, 91.98, 73.60, 56.36, 28.88, 18.83, 12.16; HRMS (ESI) m/z calcd for $C_{18}H_{17}BrN_2O_5S$ $[M + H]^+$: 453.0042 & 455.0021; found: 453.0123 & 455.0105. HPLC, t_R = 13.697 min, 98.42% purity.

N-(3-Ethyl-6-methoxybenzo[d]isoxazol-5-yl)-4-fluorobenzenesulfonamide (11o)
White solid; yield: 61.0%; m.p.: 141–142 °C; ^{1}H NMR (400 MHz, CDCl$_3$) δ 7.78 (s, 1H, 7-ArH), 7.73 – 7.64 (m, 2H, 2′, 6′-ArH), 7.10 – 7.00 (m, 2H, 3′, 5′-ArH), 6.91 (brs, 1H, SO$_2$NH), 6.85 (s, 1H, 4-ArH), 3.67 (s, 3H, OCH$_3$), 2.97 (q, J = 7.6 Hz, 2H, 3-CH$_2$CH$_3$), 1.42 (t, J = 7.6 Hz, 3H, 3-CH$_2$CH$_3$); ^{13}C NMR (101 MHz, CDCl$_3$) δ 166.52, 163.98, 161.85 (d, J = 199.0 Hz, F-4′-ArC), 159.88 (d, J = 199.0 Hz, F-4′-ArC), 153.18, 134.89 (d, J = 4.0 Hz, F-1′-ArC), 134.85 (d, J = 4.0 Hz, F-1′-ArC), 130.03 (d, J = 9.1 Hz, F-2′, 6′-ArC), 129.94 (d, J = 9.1 Hz, F-2′, 6′-ArC), 122.64, 116.14 (d, J = 22.2 Hz, F-3′, 5′-ArC), 115.92 (d, J = 22.2 Hz, F-3′, 5′-ArC), 115.19, 114.46, 92.02, 56.16, 18.87, 12.11; HRMS (ESI) m/z calcd for $C_{16}H_{15}FN_2O_4S$ $[M + H]^+$: 351.0737; found: 351.0819. HPLC, t_R = 8.228 min, 98.80% purity.

4-Chloro-N-(3-ethyl-6-methoxybenzo[d]isoxazol-5-yl) benzenesulfonamide (11p)
White solid; yield: 55.3%; m.p.: 177–178 °C; ^{1}H NMR (400 MHz, CDCl$_3$) δ 7.78 (s, 1H, 7-ArH), 7.60 (d, J = 7.4 Hz, 2H, 2′, 6′-ArH), 7.35 (d, J = 7.4 Hz, 2H, 3′, 5′-ArH), 6.92 (brs, 1H, SO$_2$NH), 6.85 (s, 1H, 4-ArH), 3.66 (s, 3H, OCH$_3$), 2.98 (d, J = 7.1 Hz, 2H, 3-CH$_2$CH$_3$), 1.43 (d, J = 6.7 Hz, 3H, 3-CH$_2$CH$_3$); ^{13}C NMR (101 MHz, CDCl$_3$) δ 161.84, 159.86, 153.15, 139.62, 137.31, 129.07 (2×C), 128.66 (2×C), 122.51, 115.18, 114.45, 92.07, 56.18, 18.88, 12.11; HRMS (ESI) m/z calcd for $C_{16}H_{15}ClN_2O_4S$ $[M + H]^+$: 367.0441; found: 367.0521. HPLC, t_R = 12.146 min, 97.73% purity.

N-(3-Ethyl-6-methoxybenzo[d]isoxazol-5-yl)-4-nitrobenzenesulfonamide (11q)
White solid; yield: 71.4%; m.p.: 168–169 °C; ^{1}H NMR (400 MHz, CDCl$_3$) δ 8.23 (d, J = 8.8 Hz, 2H, 3′, 5′-ArH), 7.87 (d, J = 8.8 Hz, 2H, 2′, 6′-ArH), 7.82 (s, 1H, 7-ArH), 7.02 (brs, 1H, SO$_2$NH), 6.86 (s, 1H, 4-ArH), 3.66 (s, 3H, OCH$_3$), 2.99 (q, J = 7.6 Hz, 2H, 3-CH$_2$CH$_3$), 1.44 (t, J = 7.6 Hz, 3H, 3-CH$_2$CH$_3$); ^{13}C NMR (101 MHz, CDCl$_3$) δ 162.02, 159.83, 153.11, 150.24, 144.62, 128.52 (2×C), 123.99 (2×C), 121.77, 115.71, 114.62, 92.26, 56.24, 18.88, 12.10; HRMS (ESI) m/z calcd for $C_{16}H_{15}N_3O_6S$ $[M + H]^+$: 378.0682; found: 378.0764. HPLC, t_R = 8.050 min, 98.64% purity.

N-(3-Ethyl-6-methoxybenzo[d]isoxazol-5-yl)-4-methoxybenzenesulfonamide (11r)
White solid; yield: 85.0%; m.p.: 145–146 °C; ^{1}H NMR (400 MHz, CDCl$_3$) δ 7.77 (s, 1H, 7-ArH), 7.61 (d, J = 8.9 Hz, 2H, 2′, 6′-ArH), 6.92 (brs, 1H, SO$_2$NH), 6.85 – 6.79 (m, 3H, 4-ArH, 3′, 5′-ArH), 3.79 (s, 3H, 6-OCH$_3$), 3.68 (s, 3H, 4′-OCH$_3$), 2.97 (q, J = 7.6 Hz, 2H, 3-CH$_2$CH$_3$), 1.42 (t, J = 7.6 Hz, 3H, 3-CH$_2$CH$_3$); ^{13}C NMR (101 MHz, CDCl$_3$) δ 163.13, 161.58, 159.88, 153.01, 130.33, 129.41 (2×C), 123.24, 114.29, 114.22, 113.89 (2×C), 91.91, 56.18, 55.59, 18.86, 12.13; HRMS (ESI) m/z calcd for $C_{17}H_{18}N_2O_5S$ $[M + H]^+$: 363.0936; found: 363.1019. HPLC, t_R = 7.687 min, 98.97% purity.

N-(3-Ethyl-6-methoxybenzo[d]isoxazol-5-yl)-4-(trifluoromethoxy) benzenesulfonamide (11s)
White solid; yield: 83.1%; m.p.: 127–128 °C; ^{1}H NMR (400 MHz, CDCl$_3$) δ 7.79 (s, 1H, 7-ArH), 7.71 (d, J = 8.8 Hz, 2H, 2′, 6′-ArH), 7.21 (d, J = 8.4 Hz, 2H, 3′, 5′-ArH), 6.88 (brs, 1H, SO$_2$NH), 6.84 (s, 1H, 4-ArH), 3.62 (s, 3H, OCH$_3$), 2.98 (q, J = 7.6 Hz, 2H, 3-CH$_2$CH$_3$), 1.43 (t, J = 7.6 Hz, 3H, 3-CH$_2$CH$_3$); ^{13}C NMR (101 MHz, CDCl$_3$) δ 162.00, 159.89, 153.38, 152.33, 137.19, 129.38 (2×C), 124.03 (q, J = 260.6 Hz, OCF$_3$), 122.33, 121.45 (q, J = 260.6 Hz, OCF$_3$), 120.64 (2×C), 118.87 (q, J = 260.6 Hz, OCF$_3$), 116.29 (q, J = 260.6 Hz, OCF$_3$), 115.91, 114.52, 92.03, 56.04, 18.88, 12.09; HRMS (ESI) m/z calcd for $C_{17}H_{15}F_3N_2O_5S$ $[M + H]^+$: 417.0654; found: 417.0732. HPLC, t_R = 18.620 min, 98.50% purity.

N-(3-Ethyl-6-methoxybenzo[d]isoxazol-5-yl)-2,4-dimethoxybenzenesulfonamide (11t)
White solid; yield: 78.2%; m.p.: 151–152 °C; ^{1}H NMR (400 MHz, CDCl$_3$) δ 7.80 – 7.72 (m, 1H, 6′-ArH), 7.70 (s, 1H, 7-ArH), 7.53 (brs, 1H, SO$_2$NH), 6.87 (s, 1H, 4-ArH), 6.45 – 6.35 (m, 2H, 3′, 5′-ArH), 3.90 (s, 3H, 2′-OCH$_3$), 3.86 (s, 3H, 6-OCH$_3$), 3.78 (s, 3H, 4′-OCH$_3$), 2.91 (q, J = 7.6 Hz, 2H, 3-CH$_2$CH$_3$), 1.36 (t, J = 7.6 Hz, 3H, 3-CH$_2$CH$_3$); ^{13}C NMR (101 MHz, CDCl$_3$) δ 165.12, 160.80, 159.82, 157.94, 152.08, 132.80, 124.03, 118.28, 114.19, 111.47, 103.99, 99.21, 91.78, 56.37, 56.05, 55.68, 18.80, 12.13; HRMS (ESI) m/z calcd for $C_{18}H_{20}N_2O_6S$ $[M + H]^+$: 393.1042; found: 393.1124. HPLC, t_R = 7.618 min, 98.26% purity.

N-(3-Ethyl-6-methoxybenzo[d]isoxazol-5-yl)-2-methoxy-4-nitrobenzenesulfonamide (11u)
White solid; yield: 57.7%; m.p.: 215–216 °C; ^{1}H NMR (400 MHz, CDCl$_3$) δ 7.99 (d, J = 8.7 Hz, 1H, 6′-ArH), 7.85 – 7.77 (m, 2H, 3′, 5′-ArH), 7.74 (s, 1H, 7-ArH), 7.59 (brs, 1H, SO$_2$NH), 6.89 (s, 1H, 4-ArH), 4.10 (s, 3H, 2′-OCH$_3$), 3.84 (s, 3H, 6-OCH$_3$), 2.93 (q, J = 7.6 Hz, 2H,

3-CH$_2$CH$_3$), 1.38 (t, J = 7.6 Hz, 3H, 3-CH$_2$CH$_3$); ^{13}C NMR (101 MHz, CDCl$_3$) δ 161.28, 159.76, 157.03, 152.38, 151.73, 132.38, 131.82, 122.60, 115.17, 114.46, 113.21, 107.04, 92.12, 56.99, 56.49, 18.81, 12.08; HRMS (ESI) m/z calcd for C$_{17}$H$_{17}$N$_3$O$_7$S [M + H]$^+$: 408.0787; found: 408.0870. HPLC, t_R = 8.697 min, 97.27% purity.

N-(3-Ethyl-6-methoxybenzo[d]isoxazol-5-yl)-3-fluoro-4-methoxybenzenesulfonamide (**11v**)
White solid; yield: 74.6%; m.p.: 203–204 °C; ^{1}H NMR (400 MHz, CDCl$_3$) δ 7.76 (s, 1H, 7-ArH), 7.55 – 7.33 (m, 2H, 2′, 6′-ArH), 6.94 (brs, 1H, SO$_2$NH), 6.91 – 6.80 (m, 2H, 4-ArH, 5′-ArH), 3.88 (s, 3H, 4′-OCH$_3$), 3.73 (s, 3H, 6-OCH$_3$), 2.97 (q, J = 7.6 Hz, 2H, 3-CH$_2$CH$_3$), 1.42 (t, J = 7.4 Hz, 3H, 3-CH$_2$CH$_3$); ^{13}C NMR (101 MHz, CDCl$_3$) δ 161.68, 159.88, 152.96, 152.70 (d, J = 252.5 Hz, F-3′-ArC), 151.74 (d, J = 10.1 Hz, F-4′-ArC), 151.64 (d, J = 10.1 Hz, F-4′-ArC), 150.20 (d, J = 252.5 Hz, F-3′-ArC), 130.65 (d, J = 6.1 Hz, F-1′-ArC), 130.59 (d, J = 6.1 Hz, F-1′-ArC), 124.73 (d, J = 4.0 Hz, F-5′-ArC), 124.69 (d, J = 4.0 Hz, F-5′-ArC), 122.82, 115.39 (d, J = 21.2 Hz, F-2′-ArC), 115.18 (d, J = 21.2 Hz, F-2′-ArC), 114.40, 112.38, 112.36, 92.05, 56.40, 56.26, 18.88, 12.13; HRMS (ESI) m/z calcd for C$_{17}$H$_{17}$FN$_2$O$_5$S [M + H]$^+$: 381.0842; found: 381.0923. HPLC, t_R = 7.802 min, 97.97% purity.

N-(3-Ethyl-6-methoxybenzo[d]isoxazol-5-yl)-3,4-dimethoxybenzenesulfonamide (**11w**)
White solid; yield: 57.9%; m.p.: 144–145 °C; ^{1}H NMR (400 MHz, CDCl$_3$) δ 7.78 (s, 1H, 7-ArH), 7.28 (dd, J = 8.5, 2.1 Hz, 1H, 6′-ArH), 7.14 (d, J = 2.1 Hz, 1H, 2′-ArH), 6.95 (brs, 1H, SO$_2$NH), 6.84 (s, 1H, 4-ArH), 6.77 (d, J = 8.5 Hz, 1H, 5′-ArH), 3.86 (s, 3H, 6-OCH$_3$), 3.76 (s, 3H, 3′-OCH$_3$), 3.69 (s, 3H, 4′-OCH$_3$), 2.96 (q, J = 7.6 Hz, 2H, 3-CH$_2$CH$_3$), 1.41 (t, J = 7.6 Hz, 3H, 3-CH$_2$CH$_3$); ^{13}C NMR (101 MHz, CDCl$_3$) δ 161.58, 159.83, 153.05, 152.78, 148.79, 130.32, 123.27, 121.36, 114.25, 114.21, 110.10, 109.48, 91.94, 56.22, 56.15, 56.10, 18.87, 12.17; HRMS (ESI) m/z calcd for C$_{18}$H$_{20}$N$_2$O$_6$S [M + H]$^+$: 393.1042; found: 393.1123. HPLC, t_R = 5.211 min, 98.56% purity.

N-(3-Ethyl-6-methoxybenzo[d]isoxazol-5-yl)-2,3-dihydrobenzofuran-5-sulfonamide (**11x**)
White solid; yield: 58.3%; m.p.: 207–208 °C; ^{1}H NMR (400 MHz, CDCl$_3$) δ 7.75 (s, 1H, 7-ArH), 7.54 – 7.46 (m, 2H, 2′, 6′-ArH), 6.92 (brs, 1H, SO$_2$NH), 6.86 (s, 1H, 4-ArH), 6.70 (d, J = 8.2 Hz, 1H, 3′-ArH), 4.61 (t, J = 8.8 Hz, 2H, OCH$_2$CH$_2$), 3.15 (t, J = 8.8 Hz, 2H, OCH$_2$CH$_2$), 2.97 (q, J = 7.6 Hz, 2H, 3-CH$_2$CH$_3$), 1.41 (t, J = 7.6 Hz, 3H, 3-CH$_2$CH$_3$); ^{13}C NMR (101 MHz, CDCl$_3$) δ 164.09, 161.47, 159.87, 152.87, 130.32, 128.94, 128.00, 124.57, 123.39, 114.29, 113.72, 109.28, 91.93, 72.28, 56.23, 28.93, 18.88, 12.15; HRMS (ESI) m/z calcd for C$_{18}$H$_{18}$N$_2$O$_5$S [M + H]$^+$: 375.0936; found: 375.1017. HPLC, t_R = 6.877 min, 98.15% purity.

N-(3-Ethyl-6-methoxybenzo[d]isoxazol-5-yl)thiophene-2-sulfonamide (**11y**)
White solid; yield: 71.4%; m.p.: 171–172 °C; ^{1}H NMR (400 MHz, CDCl$_3$) δ 7.82 (s, 1H, 7-ArH), 7.50 (dd, J = 5.0, 1.2 Hz, 1H, thiophen 5-H), 7.40 (dd, J = 3.7, 1.2 Hz, 1H, thiophen 3-H), 7.04 (brs, 1H, SO$_2$NH), 6.96 (t, J = 4.0 Hz, 1H, thiophen 4-H), 6.88 (s, 1H, 4-ArH), 3.72 (s, 3H, OCH$_3$), 2.98 (q, J = 7.6 Hz, 2H, 3-CH$_2$CH$_3$), 1.43 (t, J = 7.6 Hz, 3H, 3-CH$_2$CH$_3$); ^{13}C NMR (101 MHz, CDCl$_3$) δ 161.79, 159.93, 153.21, 139.10, 132.70, 132.51, 127.16, 122.79, 114.66, 114.35, 91.98, 56.24, 18.87, 12.14; HRMS (ESI) m/z calcd for C$_{14}$H$_{14}$N$_2$O$_4$S$_2$ [M + H]$^+$: 339.0395; found: 339.0477. HPLC, t_R = 5.799 min, 98.60% purity.

N-(3-Ethyl-6-methoxybenzo[d]isoxazol-5-yl)pyridine-3-sulfonamide (**11z**)
White solid; yield: 69.2%; m.p.: 172–173 °C; ^{1}H NMR (400 MHz, CDCl$_3$) δ 8.91 (s, 1H, pyridine 2-H), 8.72 (d, J = 4.0 Hz, 1H, pyridine 4-H), 7.92 (d, J = 8.1 Hz, 1H, pyridine 6-H), 7.81 (s, 1H, 7-ArH), 7.38 – 7.30 (m, 1H, pyridine 5-H), 7.12 (s, 1H, SO$_2$NH), 6.84 (s, 1H, 4-ArH), 3.63 (s, 3H, OCH$_3$), 2.98 (q, J = 7.6 Hz, 2H, 3-CH$_2$CH$_3$), 1.43 (t, J = 7.6 Hz, 3H, 3-CH$_2$CH$_3$); ^{13}C NMR (101 MHz, CDCl$_3$) δ 162.09, 159.85, 153.33,

153.20 (2×C), 147.92, 135.06, 123.41, 121.88, 116.21, 114.57, 92.18, 56.19, 18.86, 12.09; HRMS (ESI) m/z calcd for C$_{15}$H$_{15}$N$_3$O$_4$S [M + H]$^+$: 334.0783; found: 334.0865. HPLC, t_R = 4.186 min, 97.89% purity.

Docking studies
Preparation of the receptor. The protein (PDB ID: 5Y8Y) were prepared using the Protein Preparation Wizard within Maestro (Schrödinger, New York, NY, USA). The hydrogen atoms were added, bond orders were assigned, and missing side chains for some residues were added using Prime. The water orientations were optimized to assign H-bond using PROPKA program with the pH parameter of 7. The added hydrogens were subjected to energy minimization using OPLS3 force field.

Preparation of the ligands and molecular docking. The ligands were prepared using the LigPrep module with parameter set as no ionization. The OPLS3 force field was selected for energy minimization. The Glide docking program was used for docking studies. The grid was defined as a 20 Å box centered on the ligand. The important water molecules were kept in the binding pocket. All parameters were kept as default. No constraints were applied to all compounds except for **12**. The H-bond constraint to Asn140 was applied for the docking of scaffold **12**.

TSA assays
A 10 µL reaction mixture was added to 96-well plate. Each biochemical reaction was consisted of 1 µL of 100 µM protein, 4 µL of 500 µM compound, 1 µL of 10× fluorescent dye of SYPRO(R) orange protein gel stain (Sigma-Aldrich, Saint Louis, MO, USA), 1 µL of 10× buffer (100 mM HEPES, 1500 mM NaCl, 50% glycerin and deionized water, pH of 7.5) and 3 µL of deionized water. Total DMSO concentration was restricted to 1% or less. The 96-well plate was filmed and centrifuged at 1000 r/min for 1 min at room temperature, and then incubated on ice for 30–60 min in the dark. The plate was submitted for detection using the Bio-Rad CFX96 Real-Time PCR system (Bio-Rad, Hercules, CA, USA). The parameter of temperature range was set as 30–80 °C with a step of 0.3 °C per minute. The excitation and emission filters of the SYPRO orange dye were set at 465 nm and 590 nm, respectively. The melting temperature (T_m) was calculated by fitting the melting curve to Boltzmann equation using GraphPad Prism 5. ΔT_m represents the difference of T_m values for the tested reactions and the blank reaction. The experiments were performed in triplicates. The expression and purification of BRD4 BD1 proteins were carried out as previously described [34, 35].

Alphascreen assay
The experiment was performed according to the protocol in the previous literature [34, 35].

X-ray crystallography
Crystallization. The concentrated BRD4(1) was incubated with a 5-fold excess of compounds. A mosquito micro protein crystallizer (TTP Labtech, Royston, UK) was used for crystallization. Crystal of **11h**–BRD4(1) was grown by mixing 200 nL of the protein (12 mg/mL and 3.64 mM final ligand concentration) with 200 nL of reservoir solution containing 0.2 M ammonium sulfate, 0.1 M MES monohydrate pH 6.5, 30% w/v polyethylene glycol monomethyl ether 5,000. Crystal of **11r**–BRD4(1) was grown by mixing 200 nL of the protein (7 mg/mL and 2.12 mM final ligand concentration) with 200 nL of reservoir solution containing 0.1 M TRIS hydrochloride pH 8.5, 8% w/v polyethylene glycol 8000.

Data collection and structure solution. Data collection and structure solution were performed using a protocol from previous studies [34, 35]. Data collection and refinement statistics can be found in Table 1. The coordinates have been deposited with PDB accession codes: 7V1U for **11h**–BRD4(1), 7V2J for **11r**–BRD4(1).

Table 1. Data collection and refinement statistics for ligands and BRD4(1) complexes.

Protein/ligand	BRD4(1)/**11h**	BRD4(1)/**11r**
PDB ID	7V1U	7V2J
Space group	$P2_12_12_1$	$P2_12_12_1$
Cell dimensions		
a, b, c (Å)	35.73, 46.81, 77.38	34.22, 47.35, 77.98
α, β, γ (°)	90.00, 90.00, 90.00	90.00, 90.00, 90.00
Resolution (Å)[a]	1.82 (1.86–1.82)	2.24 (2.31–2.24)
R_{merge}[a]	0.087 (0.182)	0.092 (0.164)
$I/\sigma I$*	13.9 (5.1)	18.8 (10.6)
Completeness (%)[a]	99.9 (99.9)	99.9 (100.0)
Redundancy	8.1 (8.5)	12.4 (11.8)
R_{work}/R_{free}	0.205/0.260	0.192/0.241
No. of atoms (P/L/O)[b]	1106/25/76	1095/25/31
B_f (P/L/O) (Å^2)[b]	22.41/22.81/26.05	33.82/39.01/30.44
rms deviation bond (Å)	0.009	0.010
rms deviation angle (°)	1.486	1.415

[a]Values in brackets show the statistics for the highest resolution shells.
[b]P/L/O indicate protein, ligand, and other (water and other molecules), respectively.

Cellular anti-proliferative assay

MV4-11 cells (ATCC, Rockville, MD, USA) were cultured in IMDM supplemented with 10% FBS and 1% penicillin–streptomycin at 37 °C in a humidified incubator containing 5% CO_2. In the cell growth assay, cells were seeded in 384-well plates at 1000 cells per well in 20 µL of culture medium and cultured for 12 h. Different concentrations of diluted compounds or DMSO control were added into the wells in a volume of 10 µL with the final concentrations from 5 nM to 100 µM and cultured for 120 h. Then, 25 µL CellTiter-GLO reagent (Promega, Madison, WI, USA) was added in each well and mixed on an orbital shaker for 10 min to induce cell lysis. The lysates were incubated for another 10 min and centrifuged for 1 min. Luminescence was measured on an Enspire Multimode Plate Reader (PerkinElmer, Waltham, MA, USA), according to the manufacturer's instructions. Each concentration point was performed in triplicate. The fluorescence signals were normalized to the DMSO-treated cells, and the inhibitory curves and IC_{50} values were calculated by nonlinear regression and dose-response inhibition equation analysis using GraphPad Prism 5 software.

Quantitative real-time PCR (qRT-PCR)

Cells in the logarithmic growth phase were seeded in a 96-well plate with 5000 cells per well in 90 µL of medium, cultured for 12 h and then treated with 10 µL of different concentrations of compound. Three replicates per well for each concentration. After cultured for 48 h, the cells were harvested and washed with PBS. The total RNA was extracted by TRIzol Reagent kit (Beyotime, Shanghai, China). A 20 µL system was used for cDNA synthesis including 2 µL of RNA, 4 µL of 5× iScript reaction mix (Bio-Rad), 1 µL of iScript reverse transcriptase (Bio-Rad), and 13 µL of Nuclease-free water. The Applied Biosystems Veriti® 96-Well Thermal Cycler instrument (Thermo Fisher Scientific, Waltham, MA, USA) was used for reverse transcription with reaction at 25 °C for 5 min, 42 °C for 30 min, and 85 °C for 5 min to obtain cDNA. Then, the qRT-PCR assay was performed on the LightCycler 480 Real-Time PCR System (Roche Applied Science, Indianapolis, IN, USA) with a 20 µL reaction system, including 1 µL of cDNA, 7.4 µL of Nuclease-free water, 10 µL of SsofastEvaGreenSupermix (Bio-Rad), 0.8 µL of forward primer, 0.8 µL of reverse primer, respectively. The target mRNA expression was quantified using the $2^{-\Delta\Delta Ct}$ method and normalized to GAPDH expression. One-way ANOVA and Tukey's test were used for analysis of the statistical differences between test groups. P values < 0.05 were considered to be significantly different. The primer sequences for qPCR used are as follows: c-Myc_*fwd*, 5′-CACTAACATCCCACGCTCTGA-3′; c-Myc_*rev*, 5′-AAATCATCGCAGGCGGAACA-3′; CDK6_*fwd*, 5′-CCGAC TGACACTCGCAGC-3′; CDK6_*rev*, 5′-TCCTCGAAGCGAAGTCCTCA-3′; GA PDH_*fwd*, 5′-AATGGGCAGCCGTTAGGAAA-3′; GAPDH_*rev*, 5′-GCGCCC AATACGACCAAATC-3′.

Western blotting assay

After treatment with different concentrations of compound for 48 h, MV4-11 cells were harvested, washed by PBS, and then lysed in 400 µL of RIPA buffer (Beyotime) containing protease inhibitors PMSF (10 µL PMSF per 1 mL of RIPA) for 30 min on ice. The lysate was transferred to 1.5 mL eppendorf centrifuge tube and separated from the cell debris by centrifugation at 12,000 r/min for 5 min at 4 °C. The protein concentrations were measured using BCA Protein Assay Kit (Beyotime). Other lysate was mixed with 5× loading buffer and heated for 10 min for denaturation. The samples were separated by 8% SDS-PAGE separating gels and 4% SDS-PAGE stacking gels and then blotted into PVDF membranes (Millipore, Schwalbach, Germany). Subsequently, the PVDF membrane was washed with TBST, immersed in blocking solution (TBST solution with 5% fat-free milk) and shook at room temperature for 1 h to block the non-specific protein binding sites of PVDF membrane. The membrane was washed with TBST and then transferred to a ziplock bag. The primer antibody of anti-c-Myc antibody (ab32072, Abcam, Cambridge, UK) was diluted in a ratio of 1:1000 and incubated with the PVDF membrane at 4 °C overnight. Then, the secondary antibody Goat Anti-Rabbit IgG H&L (HRP) (ab205718, Abcam) was diluted in a ratio of 1:50000 and incubated with the PVDF membrane at room temperature for 1 h. The chemical luminescence reagent BeyoECL Plus A and B (Beyotime) was mixed in equal volume and added to the PDVF membrane. After 5 min, Tanon 6600 luminescence imaging workstation (Tanon, Shanghai, China) was used for detection. Image Pro Plus 6.0 software was used to analyze the optical density value. The tested protein levels were relative to the internal reference of GAPDH and analyzed using GraphPad Prism 5 software. One-way ANOVA and Tukey's test were used for analysis of the statistical differences between test groups. P values < 0.05 were considered to be significantly different.

Cell cycle analysis

Cells were seeded in 96-well plates at the density of 5×10^3 per well and incubated for 12 h. The gradient concentrations of compound **11r** or DMSO were added to the plates and incubated for 48 h at 37 °C. The cells were then harvested and washed with pre-cooled PBS, and then centrifuged at 10,000 r/min for 5 min at 4 °C. Cells were fixed with 500 µL 70% ethanol (v/v, 30% PBS) at 4 °C overnight and collected at 800 r/min for 15 min. Cells were washed with PBS and re-suspended in 0.4 mL PBS, and then transferred to a tube at a density of 10^6/mL. 3 µL of RNase-A was added to the tube with the final concentration of about 50 µg/mL and digested at 37 °C for 30 min. 50 µL of PI was added to the tube with the final concentration of about 65 µg/mL, and incubated on ice bath in the dark for 30 min. The cell cycle distribution was analyzed by DxFLEX flow cytometry (Beckman Coulter, Brea, CA, USA) within 1 h. The data were analyzed using Modfit LT 5.0 software and quantified by GraphPad Prism 5 software. One-way ANOVA and Tukey's test were used for analysis of the statistical differences between test groups. P values < 0.05 were considered to be significantly different.

Apoptosis analysis

Cells were collected and washed with 4 °C pre-cooled PBS, and then centrifuged at 10,000 r/min for 5 min at 4 °C. The cells was re-suspended in 1× Annexin binding buffer with the density of 10^6/ mL. 5 µL Alexa Fluor 488 Annexin V and 1 µL 100 µg/mL propidium
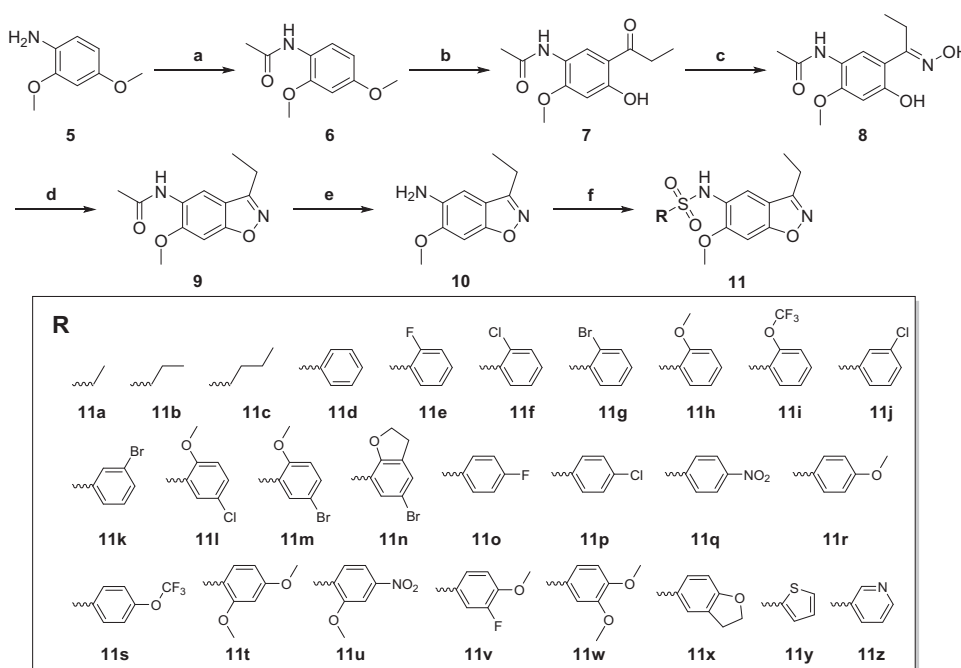
Scheme 1 The synthetic route of 3-ethyl-benzo[d]isoxazole containing sulfonamide derivatives. Reagents and conditions: (**a**) Acetic anhydride, triethylamine, DCM, rt, 88%; (**b**) Propionyl chloride, AlCl$_3$, DCM, 43 °C, 81%; (**c**) Hydroxylamine hydrochloride, sodium acetate, EtOH/H$_2$O, 80 °C, 86%; (**d**) DMF-DMA, 1,4-dioxane, 100 °C, 56%; (**e**) HCl/H$_2$O, 90 °C, 93%; (**f**) Sulfonyl chlorides, pyridine, DCM, 43 °C, 39%–85%.

iodide (PI) working solution (Invitrogen, Carlsbad, CA, USA) were added to each 100 µL cell suspension and incubated at room temperature for 15 min in dark and analyzed by flow cytometry. The data were analyzed using the workstation for flow cytometry (Beckman) and quantified by GraphPad Prism 5 software. One-way ANOVA and Tukey's test were used for analysis of the statistical differences between test groups. P values < 0.05 were considered to be significantly different.

RESULTS

Chemistry

The target compounds were synthesized in a tandem six steps with the commercially available 2,4-dimethoxyaniline as the starting material (Scheme 1). In the first step, the amino group of compound **5** was acetylated with acetic anhydride to obtain compound **6**. Next, a propionyl group was introduced on the benzene ring of **6** via anhydrous AlCl$_3$ mediated Friedel-Crafts reaction, which afforded compound **7**. The methoxy group at the ortho position of the carbonyl group was selectively removed to give the hydroxyl group. Compound **7** was reacted with hydroxylamine hydrochloride to generate the oxime intermediate **8**. The intermediate **8** was submitted to cyclization at high temperature in the presence of DMF-DMA to give isoxazole derivative **9**, which was then hydrolyzed by hydrochloric acid to give the scaffold **10**. The target compounds **11a–z** were finally synthesized in a one-plot step through the reaction of compound **10** with different sulfonyl chlorides.

Biological activity

SAR studies against BRD4. The X-ray crystallographic structure of **4**-BRD4(1) complex (PDB: 5Y8Y) previously reported by our laboratory provided solid evidence for the structure-based optimization in this work. We initially docked the scaffolds **10** (3-ethyl-6-methoxybenzo[d]isoxazol-5-amine) and **12 (**3-methyl-6-methoxybenzo[d]isoxazol-5-amine) into the bromodomain of BRD4. Both scaffolds resided into the K$_{Ac}$ binding site and the

3-ethyl on scaffold **10** could occupy more space in the sub-pocket than 3-methyl group (**12**) (Fig. 2). The binding advantage was also supported by the two docking scores (−7.2 & −39 vs −6.6 & −35) (Supplementary Table S1). Next, many compounds containing the 3-ethyl-6-methoxybenzo[d]isoxazol-5-amine core were designed and submitted to molecular docking before synthesis (Supplementary Table S1). The two scoring models such as docking score and glide emodel score were used as the preliminary screening reference indicators. Compounds with docking score < −7.1 and glide emodel score < −55 would be synthesized and tested.

All the synthesized small molecules were evaluated by the TSA screening method against BRD4(1) (Table 2). Firstly, an ethyl group (**11a**) was introduced at R position, which showed moderate binding activity to BRD4. Extending the alkyl chain to 3 carbon atoms (**11b**) or 4 carbon atoms (**11c**) led to increased activities with ΔT_m values of 6.5 °C and 7.2 °C, respectively.

Next, phenyl groups were introduced at R position. The unsubstituted phenyl compound **11d** exhibited moderate activity. The introduction of small groups such as F (**11e**), Cl (**11f**), Br (**11g**), OCH$_3$ (**11h**), OCF$_3$ (**11i**) to the 2′ position of benzene ring led to increased activities. Among which, the 2′-OCH$_3$ substituted compound **11h** showed the most potent binding activity with thermal shift value of 8.0 °C. The 2′-OCF$_3$ also showed increased activity compared with **11e–g** and slightly decreased activity versus **11h**. Parallel results showed that the introduction of small groups at the 3′ position of benzene ring still maintained slightly stronger activities (**11f** vs **11j**; **11g** vs **11k**). Compounds with 2′ and 3′ multi-substitutions (**11l–n**) were also designed and synthesized. The compounds showed ΔT_m values of 6.0–6.6 °C, which were slightly lower than that of **11h**.

To further detail the structure-activity relationships, we investigated the impact of substitutions at the 4′ position of the benzene ring (Table 3). The results for compounds **11o–p** indicated that 4′-F and 4′-Cl were tolerated on the phenyl ring, with similar ΔT_m values against BRD4 compared to 2′ substitution (**11e** & **11f**). The introduction of the strongly electron-withdrawing nitro group in compound **11q** showed an increased activity. The
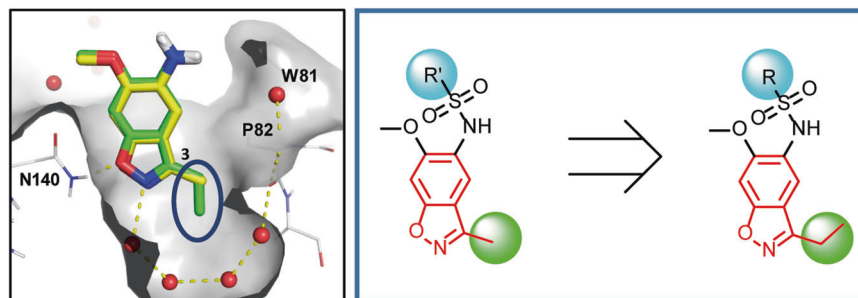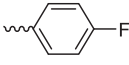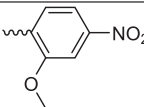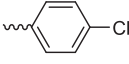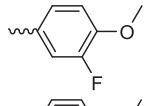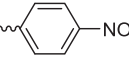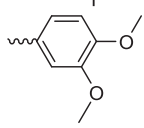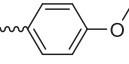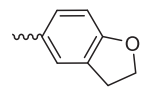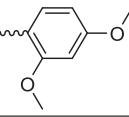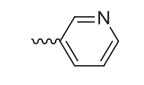
Fig. 2 Structure–based design of new benzo[d]isoxazole derivatives. Green sticks: compound **10**, yellow sticks: compound **12**.

Table 2. Binding activities of compounds **11a-n** against BRD4.
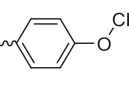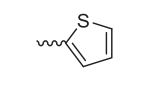
No.	R	TSA ΔT_m (°C)	No.	R	TSA ΔT_m (°C)
4	-	6.4	**11h**		8.0
11a		3.9	**11i**		6.8
11b		6.5	**11j**		6.2
11c		7.2	**11k**		6.0
11d		5.1	**11l**		6.5
11e		6.0	**11m**		6.5
11f		5.9	**11n**		6.0
11g		5.7			

Table 3. Binding activities of compounds **11o-z** against BRD4.

No.	R	TSA ΔT_m (°C)	No.	R	TSA ΔT_m (°C)
11o	⟶⟨benzene⟩–F	5.9	**11u**	⟶⟨benzene, O, NO₂⟩	7.5
11p	⟶⟨benzene⟩–Cl	5.5	**11v**	⟶⟨benzene, O, F⟩	1.5
11q	⟶⟨benzene⟩–NO₂	6.3	**11w**	⟶⟨benzene, O, O⟩	4.5
11r	⟶⟨benzene⟩–O	6.2	**11x**	⟶⟨dihydrobenzofuran⟩	6.0
11s	⟶⟨benzene⟩–O–CF₃	4.0	**11y**	⟶⟨thiophene⟩	5.7
11t	⟶⟨benzene, O, O⟩	6.5	**11z**	⟶⟨pyridine⟩	6.8

Fig. 3 The inhibitory effect of compounds against BRD4(1). The inhibitory curves and the half-maximum inhibitory concentration (IC₅₀) values for all compounds against BRD4(1) were obtained from the alphascreen assay.

No.	11c	11h	11i	11r	11t	11u	4
IC₅₀ (μM)	0.26	0.094	0.30	0.67	0.89	1.21	0.048

compound **11r** with electron-donating 4'-OCH₃ group displayed similar activity compared to **11q**. Analog **11s** showed a decreased activity versus **11r**.

To identify more potent inhibitors, multi-substituted compounds at 2' and 4' positions or at 3' and 4' positions were synthesized. Since the 2'- or 4'- methoxy groups showed better activities, we retained the above groups in the synthesis of **11t-x**. Among them, compounds **11t**, **11u**, **11x** exhibited potent activities with ΔT_m values of 6.5, 7.5, 6.0 °C, respectively. We also introduced two heterocyclic motifs as R groups, which afforded **11y** and **11z** with good binding activities.

The IC₅₀ values for several representative compounds were further determined by alphascreen method. Most compounds exhibited nanomolar activities (Fig. 3). Among which, **11h** exhibited the most potent activity with an IC₅₀ value of 0.094 μM.

We also successfully obtained two crystal structures. The binding modes of compounds 11h and 11r in complex with BRD4 (1) were determined by X-ray crystallography and illustrated in Fig. 4. Multiple hydrogen bond interactions were observed between the compounds and the protein or the water network. The 3-ethyl-benzo[d]isoxazole cores shared the similar binding pattern in both compounds with the oxygen forming a hydrogen bond to Asn140 and the nitrogen forming a hydrogen bond to the NO.1 conserved water molecule (Fig. 4a). The 2'-OCH₃ of **11h** formed a hydrogen bond to NO.9 solvent water molecule, which further bound to Leu92 (Fig. 4b). The 4'-OCH₃ of **11r** formed a hydrogen bond to NO.8 water molecule, which further bound to Ile146 (Fig. 4c). The benzene rings attached to sulfonamides in both compounds were not fully overlapped with each other (Fig. 4d). The 4' carbon atom of **11r** shifted 1.3 Å toward the orientation of No. 8 water molecule compared with **11h**, probably to form a more stable H-bond (Supplementary Fig. S2a). This shift of **11r** further induced the nearby amino residues such as Asp145 and Trp81 to shift 0.8 Å and 0.5 Å, respectively.

The crystal structures of **11h**, **11r**, **3** and **4** were also superimposed. All the scaffolds in the four compounds shared similar binding modes to mimic the K_Ac (Supplementary Fig. S2b). The benzene rings of **11h** and **3** were overlapped well with each other in the WPF region (Fig. 4e, Supplementary Fig. S2c). Besides, the benzene rings of **11r** and **4** were also completely overlapped (Fig. 4f, Supplementary Fig. S2c).

Selectivity evaluation

TSA assay was performed for representative compounds against 11 bromodomain-containing proteins. All compounds exhibited binding activities with ΔT_m of 6.2–8.0 °C for BRD4(1) and 3.8–5.8 °C for BRD3(1) (Table 4). Besides, the compounds also showed activities with ΔT_m of 1.5–4.5 °C for BRD2(2) and BRDT(1). No thermal shifts were observed in other proteins.
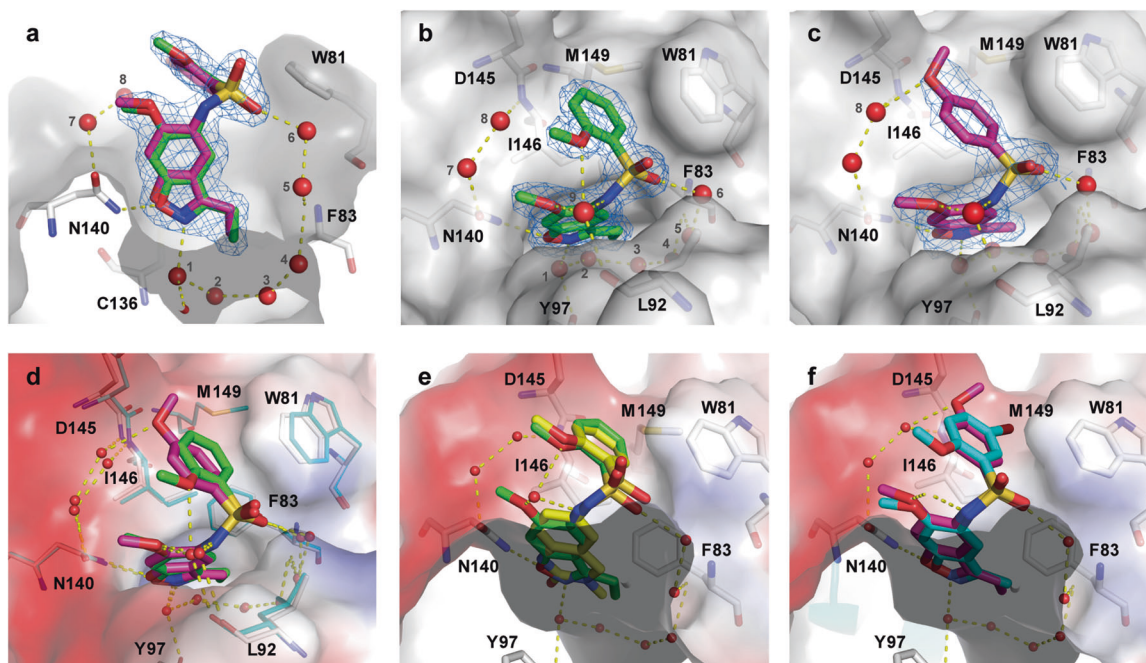
Fig. 4 X-ray crystal structures of representative compounds 11h (green sticks) and 11r (magentas sticks) in complex with BRD4(1) (PDB ID: 7V1U for 11h, 7V2J for 11r; protein, gray surface; key residues, thin sticks; water molecules, red spheres; hydrogen bonds, yellow dashed lines; electron density, blue grid). **a** Superimposed crystal structures of **11h** and **11r** in complex with BRD4(1). The 3-ethyl-benzo[d] isoxazole cores of compounds share the similar poses in the KAc binding pocket. **b** X-ray crystal structure of **11h** bound to BRD4(1). **c** X-ray crystal structure of **11r** bound to BRD4(1). **d** Superimposed crystal structures of **11h** (cyan thin sticks for protein residues) and **11r** (gray thin sticks for protein residues) bound to BRD4(1), with the phenyls occupying on the WPF shelf. **e** Superimposed crystal structures of **11h** and **3** (PDB ID: 4E96, yellow stick) in complex with BRD4(1). **f** Superimposed crystal structures of **11r** and **4** (PDB ID: 5Y8Y, cyan stick) in complex with BRD4(1). The vacuum electrostatic surface of BRD4(1) was generated by pymol.

Table 4. Selectivity evaluation for representative compounds against 11 bromodomain-containing proteins by thermal shift assay.

Protein	ΔT_m (°C)[a]			
	4	11h	11r	11t
BRD4(1)	6.4	8.0	6.2	6.5
BRD2(2)	3.6	4.5	2.5	3.6
BRD3(1)	4.3	5.8	3.8	4.3
BRDT(1)	2.5	3.5	1.5	1.5
BRD9	-0.3	-0.4	-0.4	-0.6
BAZ2B	0.2	0.1	-0.1	-0.1
BRD1	0.4	-0.3	0.1	0.1
TAF1(1)	0.3	0.2	-0.1	-0.3
ASH1L	0.3	-0.5	-0.3	-1.5
EP300	1.3	-0.3	-0.3	-0.8
CREBBP	0.7	0.0	0.6	-0.1

[a]The heat map shows the relative ΔT_m, where red indicates a large ΔT_m.

Inhibitory activity against AML cells

Several compounds were selected for evaluation of the inhibitory effect against human AML cells MV4-11. Compound **4** was included as a positive control. After the treatment with compounds for 120 h, the proliferation of MV4-11 cells were inhibited in a dose-dependent manner (Fig. 5). Compounds **11h** and **11r** showed nanomolar inhibitory activities with EC$_{50}$ values

of 0.78 μM and 0.87 μM. Other selected compounds also exhibited good inhibitory activities with EC$_{50}$ values ranging from 2.5 μM to 5.5 μM.

### Inhibition on the expression of BRD4 downstream genes

To further confirm the anti-proliferative mechanism of inhibitors, the real-time quantitative PCR and western blot assays were performed to detect the level of target genes in MV4-11 cells effected by representative compounds. As the research on the biological mechanism of **11h** was still in progress, only the results of **11r** were reported here. The mRNA expression of c-Myc and CDK6 in MV4-11 decreased significantly in the compound **11r** treatment group (1 μM, 5 μM and 10 μM) compared with the control group (Fig. 6). In addition, a remarkable dose-dependent decrease of c-Myc expression was observed at the protein level (Fig. 7).

Flow cytometry analysis

To further investigate the mechanism of anti-proliferative effects, we employed flow cytometry analysis to evaluate the ability of compound **11r** for induction of cell cycle arrest and apoptosis in the MV4-11 cell lines. In cell cycle analysis assay, compound **11r** could induce cell cycle arrest in G$_0$/G$_1$ phase in a dose-dependent manner (Fig. 8). The apoptosis rate of **11r** (1 μM, 5 μM and 10 μM) treated groups was significantly increased compared with the control group (Fig. 9).

DISCUSSION

We previously reported a class of BET inhibitors containing a 3-methyl-6-methoxybenzo[d]isoxazol scaffold [35]. Molecular docking studies revealed similar binding advantage for 3-ethyl-substituted backbone (Fig. 2). This led to the design of compounds containing the 3-ethyl-6-methoxybenzo[d]isoxazol-5-

No.	EC$_{50}$ (μM)	No.	EC$_{50}$ (μM)
4	0.85	11r	0.87
11c	2.50	11t	2.50
11h	0.78	11u	3.79
11i	5.53		
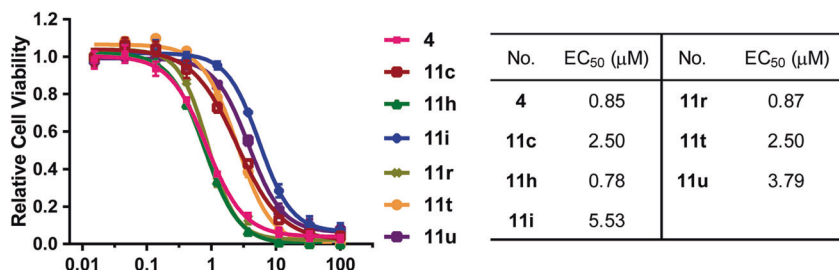
Fig. 5 Inhibition of cell proliferation of compounds against the MV4-11 cell lines. CellTiter-Glo was used to detect the viability after the treatment of the indicated concentrations of compounds for 120 h.
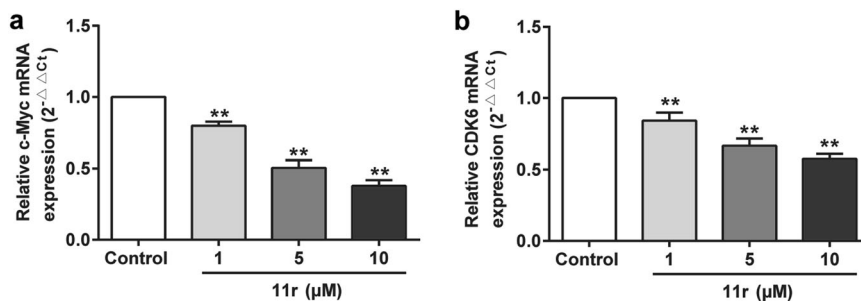
Fig. 6 Effect of the mRNA expressions of c-Myc and CDK6 in MV4-11. The mRNA levels of c-Myc (**a**) and CDK6 (**b**) were detected by RT-PCR. The mRNA levels of c-Myc and CDK6 were normalized to control. The results were presented as mean ± SD ($n = 3$). **$P < 0.01$, vs. control group.
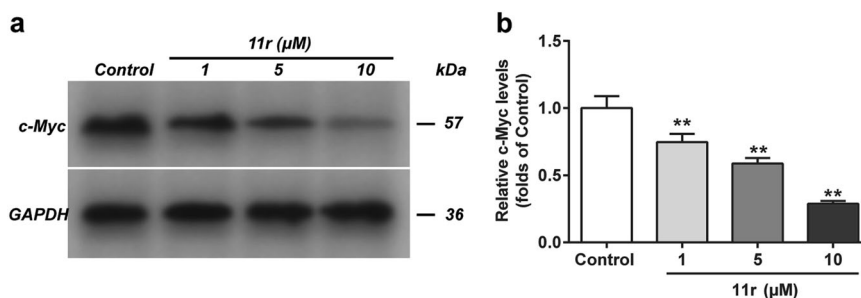

Fig. 7 The level of c-Myc expression in MV4-11. a The representative bands for different treatment groups were detected by Western blot assay. **b** The quantification of the expression levels of c-Myc. The levels of c-Myc were normalized to control. The results were presented as mean ± SD ($n = 3$).

amine core, which we would like to explore the chemical space and investigate the more detailed structure-activity relationships against BRD4.

As the sulfonamide is an effective linker for attaching the substituent to occupy the WPF shelf region [29, 34, 35], we initially retained the sulfonamide while changing the R groups. The results were consistent with the previous data [35] that lipophilic substituent of three to five heavy atoms was acceptable for occupying the WPF region. Since the benzene ring is also a lipophilic substituent, the substituted or unsubstituted phenyl groups were introduced at R position. The data suggested that the 2' and 3' positions of the benzene were tolerated for substitution. Besides, the 4' position of the phenyl ring was also tolerated for modification, which was different from the previous SAR studies [35]. Moreover, the heterocycle was also tolerated for substitution and can be further modified to generate potent inhibitors.

The TSA assay evaluates the binding affinity under the condition of excess compound to protein concentration ratio (20:1). In order to investigate the binding ability of the compound to the protein at different concentrations, alphascreen assays were performed for representative compounds. The results further confirmed the potent activities of all the selected compounds (Fig. 3).

In the early stage of the research, molecular docking technology was used for the guidance of drug design. However, the real binding modes of small molecules and proteins were still worthy of exploration. Two crystal structures of compounds **11h** and **11r** in complex with BRD4(1) were obtained. Both compounds exhibited similar binding mode with the 3-ethyl-benzo[d]isoxazole core residing into the K$_{Ac}$ binding pocket (Fig. 4a). The 9 water molecules and proteins formed a water network as previously reported [35]. The electron density maps of both compounds showed excellent shape complementary with the protein binding pocket. The crystal structures of **11h** and **11r** were also superimposed with the two structural related compounds **3** and **4** for comparison. It was noteworthy that the 3-ethyl on the scaffolds of **11h** and **11r** extended deeper to inner sub-pocket as we expected compared with **4** (Supplementary Fig. S2b). However, the four compounds adopted two sets of binding modes with nuance in the WPF region. The results indicated that substitutions at the 4' or 5' positions of the benzene ring would push the benzene ring to the side away from Trp81. We originally thought that the benzene ring was bound at the same position and then the binding potency may be improved by adding substituents to the benzene ring. The results may explain why the activities of multi-substituted compounds were not improved.
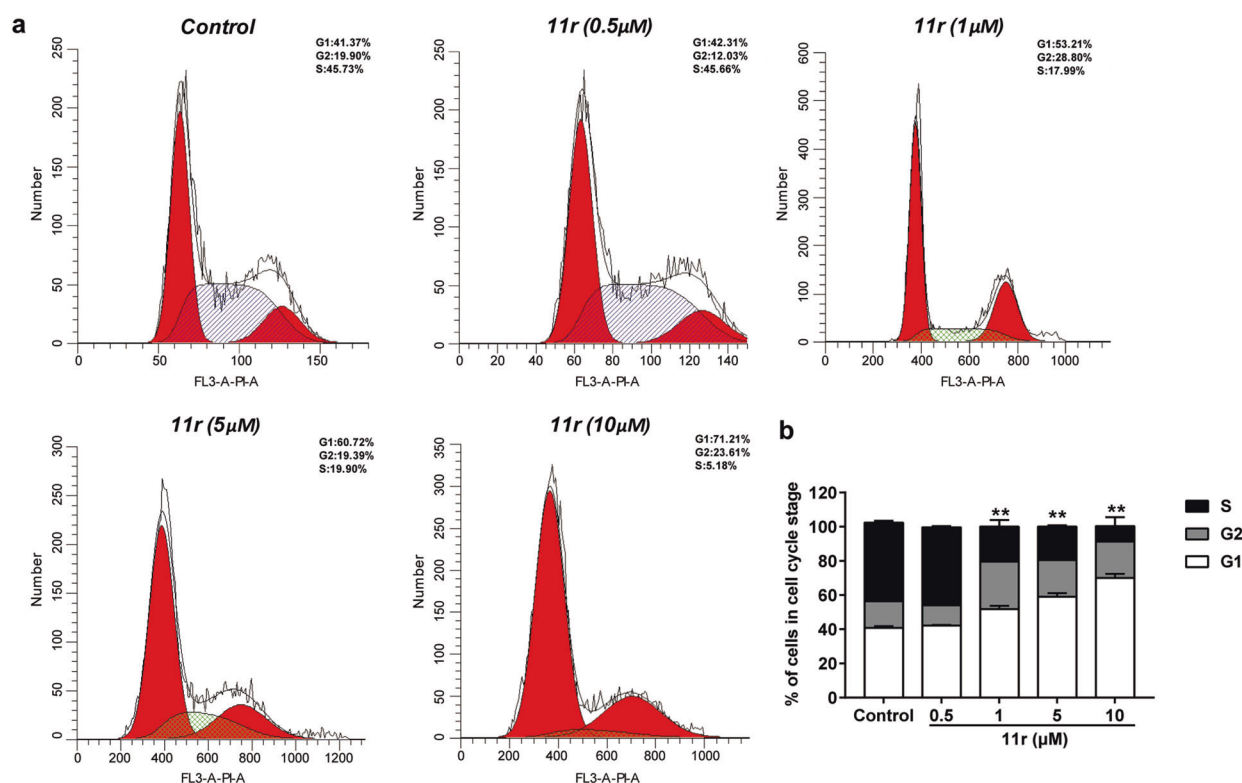
Fig. 8 MV4-11 cells were arrested at G_1 phase by 11r. a Flow cytometry analysis of the distribution of cell cycle in MV 4-11 cells after treatment of DMSO and the indicated concentrations of compound **11r**. Propidium iodide was used for staining of MV4-11. **b** The quantification of the analysis of cell cycle phase. Results were mean ± SD for 3 individual experiments which, for each condition, were repeated 3 times. **$P < 0.01$, vs. control group.
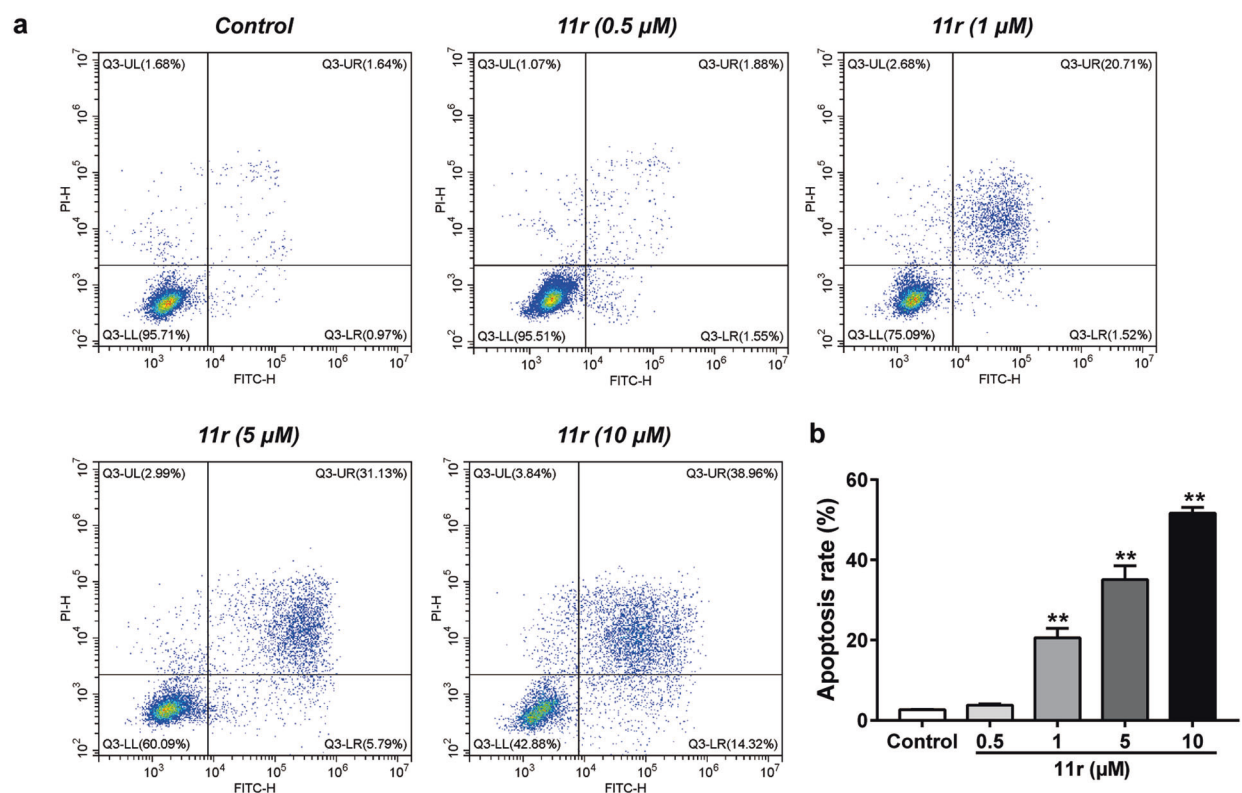
Fig. 9 Compound 11r induced apoptosis in MV4-11 cells. a MV4-11 cells were treated with different concentrations of **11r**, then apoptosis in MV4-11 cells was assessed by flow cytometer analysis after staining with AnnexinV and PI. **b** The quantification of the apoptosis rate in MV4-11 cells. Results were mean ± SD for 3 individual experiments which, for each condition, were repeated 3 times. **$P < 0.01$, vs. control group.

The crystal structures were also overlaid with the docked structures for comparison. The crystal structure of **11h** exhibited the similar binding mode compared to the docked structure (Supplementary Fig. S2d). However, the crystal structure of **11r** was obviously different from the docked structure in the poses of the phenyl substitution (Supplementary Fig. S2e). We deemed that the 4′-substituted phenyl compounds would cause the surrounding Asp145 to shift flexibly when they bound to the protein. However, Asp145 was not shifted flexibly to accommodate the small molecules in conventional molecular docking process, which generated the inaccurate binding mode. Overall, the obtained crystal structures further confirmed the high binding affinities of small molecules to proteins.

The bromodomains are structurally conserved modules and are present in a variety of proteins. To evaluate the selectivity profile of compounds, 11 bromodomain-containing proteins from different families were selected for testing. The results indicated that all compounds exhibited excellent selectivity for BET family of bromodomains over other protein members (Table 4). Although the reference compound **4** showed weak activity for EP300 with ΔT_m of 1.25 °C, other synthesized compounds showed less activity for this protein.

Much evidence showed that BRD4 played important roles in the development of acute myeloid leukemia [6, 8, 9]. Therefore, we evaluated the anti-proliferative effect of representative compounds against AML cells MV4-11. Compounds **11h** (0.78 μM) and **11r** (0.87 μM) showed similar inhibitory activities compared to positive compound **4** (0.85 μM). Combined data indicated that the cellular inhibitory activities were mainly caused by the inhibition of BET bromodomains. As an epigenetic reader of acetyl lysine, BRD4 participated in the regulation of specific gene expression including c-Myc and CDK6 in AML [6, 37]. Compound **11r** concentration-dependently inhibited the expression levels of oncogenes including c-Myc and CDK6 in MV4-11 cells. The results showed that the compound inhibited the expression of downstream oncogenes by inhibiting the BET bromodomains. Moreover, flow cytometry analysis indicated that **11r** concentration-dependently blocked cell cycle in MV4-11 cells at G_0/G_1 phase and induced cell apoptosis.

CONCLUSIONS
In summary, based on our previously reported BRD4 inhibitors, a new series of 3-ethyl-benzo[d]isoxazole derivatives were designed and synthesized as BRD4 inhibitors under the guidance of molecular docking studies. The detailed SARs indicated that 3-ethyl was acceptable for the sub-pocket. Further exploration also indicated that the 4′ position of the phenyl ring was tolerated for modification. The actual binding modes of potent compounds **11h** and **11r** were disclosed by the X-ray cocrystal structures. Among the 26 synthesized compounds, compound **11h** and **11r** were potent inhibitors against BRD4 and showed strong anti-proliferative effect against human leukemia cell lines MV4-11. In the RT-PCR and Western blot assay, compound **11r** could decrease the transcription or expressions of c-Myc and CDK6 in MV4-11 cell. In addition, **11r** was able to induce cell cycle arrest at G_0/G_1 phase and induce cell apoptosis. The results indicated that N-(3-ethylbenzo[d]isoxazol-5-yl)sulfonamide derivative **11r** is a promising lead compound and can be used to further explore drug candidate.

AUTHOR CONTRIBUTIONS
YX, MFZ, YZ and XYL designed the study. MFZ, CZ, CW, XSW, and QPX performed the experiments. MFZ and XYL wrote the manuscript. YX, MFZ, YZ and XYL revised the manuscript. All authors reviewed the results and approved the final version of the manuscript.

ADDITIONAL INFORMATION
Supplementary information The online version contains supplementary material available at https://doi.org/10.1038/s41401-022-00881-y.

Competing interests: The authors declare no competing interests.

REFERENCES
1. Arrowsmith CH, Bountra C, Fish PV, Lee K, Schapira M. Epigenetic protein families: a new frontier for drug discovery. Nat Rev Drug Discov. 2012;11:384–400.
2. Wu SY, Chiang CM. The double bromodomain-containing chromatin adaptor Brd4 and transcriptional regulation. J Biol Chem. 2007;282:13141–5.
3. Romero FA, Taylor AM, Crawford TD, Tsui V, Cote A, Magnuson S. Disrupting acetyl-lysine recognition: progress in the development of bromodomain inhibitors. J Med Chem. 2016;59:1271–98.
4. Shi J, Vakoc CR. The mechanisms behind the therapeutic activity of BET bromodomain inhibition. Mol Cell. 2014;54:728–36.
5. Donato E, Croci O, Sabo A, Muller H, Morelli MJ, Pelizzola M, et al. Compensatory RNA polymerase 2 loading determines the efficacy and transcriptional selectivity of JQ1 in Myc-driven tumors. Leukemia. 2017;31:479–90.
6. Dawson MA, Prinjha RK, Dittmann A, Giotopoulos G, Bantscheff M, Chan W-I, et al. Inhibition of BET recruitment to chromatin as an effective treatment for MLL-fusion leukaemia. Nature. 2011;478:529–33.
7. Delmore JE, Issa GC, Lemieux ME, Rahl PB, Shi J, Jacobs HM, et al. BET bromodomain inhibition as a therapeutic strategy to target c-Myc. Cell. 2011;146:904–17.
8. Zuber J, Shi JW, Wang E, Rappaport AR, Herrmann H, Sison EA, et al. RNAi screen identifies Brd4 as a therapeutic target in acute myeloid leukaemia. Nature. 2011;478:524–8.
9. Reyes-Garau D, Ribeiro LM, Roué G. Pharmacological targeting of BET bromodomain proteins in acute myeloid leukemia and malignant lymphomas: from molecular characterization to clinical applications. Cancers. 2019;11:1483.
10. Latif AL, Newcombe A, Li S, Gilroy K, Robertson NA, Lei X, et al. BRD4-mediated repression of p53 is a target for combination therapy in AML. Nat Commun. 2021;12:241.
11. Asangani IA, Dommeti VL, Wang XJ, Malik R, Cieslik M, Yang RD, et al. Therapeutic targeting of BET bromodomain proteins in castration-resistant prostate cancer. Nature. 2014;510:278–82.
12. Faivre EJ, McDaniel KF, Albert DH, Mantena SR, Plotnik JP, Wilcox D, et al. Selective inhibition of the BD2 bromodomain of BET proteins in prostate cancer. Nature. 2020;578:306–10.
13. Shu SK, Lin CY, He HH, Witwicki RM, Tabassum DP, Roberts JM, et al. Response and resistance to BET bromodomain inhibitors in triple-negative breast cancer. Nature. 2016;529:413–7.
14. Tian Y, Wang X, Zhao S, Liao X, Younis MR, Wang S, et al. JQ1-loaded polydopamine nanoplatform inhibits c-MYC/programmed cell death ligand 1 to enhance photothermal therapy for triple-negative breast cancer. ACS Appl Mater Interfaces. 2019;11:46626–36.
15. Chang X, Sun D, Shi D, Wang G, Chen Y, Zhang K, et al. Design, synthesis, and biological evaluation of quinazolin-4(3H)-one derivatives co-targeting poly(ADP-ribose) polymerase-1 and bromodomain containing protein 4 for breast cancer therapy. Acta Pharm Sin B. 2021;11:156–80.
16. Mu J, Sun P, Ma Z, Sun P. BRD4 promotes tumor progression and NF-κB/CCL2-dependent tumor-associated macrophage recruitment in GIST. Cell Death Dis. 2019;10:935.

17. Huang M, Zeki J, Sumarsono N, Coles GL, Taylor JS, Danzer E, et al. Epigenetic targeting of TERT-associated gene expression signature in human neuroblastoma with TERT overexpression. Cancer Res. 2020;80:1024–35.

18. He S, Dong G, Li Y, Wu SY, Wang W, Sheng C. Potent dual BET/HDAC inhibitors for efficient treatment of pancreatic cancer. Angew Chem Int Ed. 2020;59:3028–32.

19. Leal AS, Liu P, Krieger-Burke T, Ruggeri B, Liby KT. The bromodomain inhibitor, INCB057643, targets both cancer cells and the tumor microenvironment in two preclinical models of pancreatic cancer. Cancers. 2021;13:96.

20. Fehling SC, Miller AL, Garcia PL, Vance RB, Yoon KJ. The combination of BET and PARP inhibitors is synergistic in models of cholangiocarcinoma. Cancer Lett. 2020;468:48–58.

21. Nicodeme E, Jeffrey KL, Schaefer U, Beinke S, Dewell S, Chung CW, et al. Suppression of inflammation by a synthetic histone mimic. Nature. 2010;468:1119–23.

22. Jiang F, Hu Q, Zhang Z, Li H, Li H, Zhang D, et al. Discovery of benzo[cd]indol-2(1H)-ones and pyrrolo[4,3,2-de]quinolin-2(1H)-ones as bromodomain and extra-terminal domain (BET) inhibitors with selectivity for the first bromodomain with potential high efficiency against acute gouty arthritis. J Med Chem. 2019;62:11080–107.

23. Filippakopoulos P, Qi J, Picaud S, Shen Y, Smith WB, Fedorov O, et al. Selective inhibition of BET bromodomains. Nature. 2010;468:1067–73.

24. Berthon C, Raffoux E, Thomas X, Vey N, Gomez-Roca C, Yee K, et al. Bromodomain inhibitor OTX015 in patients with acute leukaemia: a dose-escalation, phase 1 study. Lancet Haematol. 2016;3:e186–95.

25. Mirguet O, Gosmini R, Toum J, Clément CA, Barnathan M, Brusq JM, et al. Discovery of epigenetic regulator I-BET762: lead optimization to afford a clinical candidate inhibitor of the BET bromodomains. J Med Chem. 2013;56:7501–15.

26. Hewings DS, Wang M, Philpott M, Fedorov O, Uttarkar S, Filippakopoulos P, et al. 3,5-Dimethylisoxazoles act as acetyl-lysine-mimetic bromodomain ligands. J Med Chem. 2011;54:6761–70.

27. Zhao Y, Bai L, Liu L, McEachern D, Stuckey JA, Meagher JL, et al. Structure-based discovery of 4-(6-methoxy-2-methyl-4-(quinolin-4-yl)-9h-pyrimido[4,5-b]indol-7-yl)-3,5-dimethylisoxazole (CD161) as a potent and orally bioavailable BET bromodomain inhibitor. J Med Chem. 2017;60:3887–901.

28. Xue X, Zhang Y, Wang C, Zhang M, Xiang Q, Wang J, et al. Benzoxazinone-containing 3,5-dimethylisoxazole derivatives as BET bromodomain inhibitors for treatment of castration-resistant prostate cancer. Eur J Med Chem. 2018;152:542–59.

29. Fish PV, Filippakopoulos P, Bish G, Brennan PE, Bunnage ME, Cook AS, et al. Identification of a chemical probe for bromo and extra C-terminal bromodomain inhibition through optimization of a fragment-derived hit. J Med Chem. 2012;55:9831–7.

30. Altenburg B, Frings M, Schöbel J-H, Goßen J, Pannen K, Vanderliek K, et al. Chiral analogues of PFI-1 as BET inhibitors and their functional role in myeloid malignancies. ACS Med Chem Lett. 2020;11:1928–34.

31. Zhao L, Wang Y, Cao D, Chen T, Wang Q, Li Y, et al. Fragment-based drug discovery of 2-thiazolidinones as BRD4 inhibitors: 2. structure-based optimization. J Med Chem. 2015;58:1281–97.

32. McDaniel KF, Wang L, Soltwedel T, Fidanze SD, Hasvold LA, Liu D, et al. Discovery of n-(4-(2,4-difluorophenoxy)-3-(6-methyl-7-oxo-6,7-dihydro-1h-pyrrolo[2,3-c]pyridin-4-yl)phenyl)ethanesulfonamide (ABBV-075/mivebresib), a potent and orally available bromodomain and extraterminal domain (BET) family bromodomain inhibitor. J Med Chem. 2017;60:8369–84.

33. Albrecht BK, Gehling VS, Hewitt MC, Vaswani RG, Cote A, Leblanc Y, et al. Identification of a benzoisoxazoloazepine inhibitor (CPI-0610) of the bromodomain and extra-terminal (BET) family as a candidate for human clinical trials. J Med Chem. 2016;59:1330–9.

34. Xue XQ, Zhang Y, Liu ZX, Song M, Xing YL, Xiang QP, et al. Discovery of benzo[cd]indol-2(1H)-ones as potent and specific BET bromodomain inhibitors: structure-based virtual screening, optimization, and biological evaluation. J Med Chem. 2016;59:1565–79.

35. Zhang M, Zhang Y, Song M, Xue X, Wang J, Wang C, et al. Structure-based discovery and optimization of benzo[d]isoxazole derivatives as potent and selective BET inhibitors for potential treatment of castration-resistant prostate cancer (CRPC). J Med Chem. 2018;61:3037–58.

36. Mita MM, Mita AC. Bromodomain inhibitors a decade later: a promise unfulfilled? Br J Cancer. 2020;123:1713–4.

37. Feng Y, Xiao S, Chen Y, Jiang H, Liu N, Luo C, et al. Design, synthesis and biological evaluation of benzo[cd]indol-2(1H)-ones derivatives as BRD4 inhibitors. Eur J Med Chem. 2018;152:264–73.